SPACE RADIATION ENVIRONMENT AND RADIATION HARDNESS ASSURANCE TESTS OF ELECTRONIC COMPONENTS TO BE USED IN SPACE MISSIONS

A THESIS SUBMITTED TO
THE GRADUATE SCHOOL OF NATURAL AND APPLIED SCIENCES
OF
MIDDLE EAST TECHNICAL UNIVERSITY

BY

ÖZGE AMUTKAN

IN PARTIAL FULFILLMENT OF THE REQUIREMENTS
FOR
THE DEGREE OF DOCTOR OF PHILOSOPHY
IN
PHYSICS

JULY 2010

Approval of the thesis:

SPACE RADIATION ENVIRONMENT AND RADIATION HARDNESS ASSURANCE TESTS OF ELECTRONIC COMPONENTS TO BE USED IN SPACE MISSIONS

submitted by **ÖZGE AMUTKAN** in partial fulfillment of the requirements for the degree of **Doctor of Philosophy in Physics Department, Middle East Technical University** by,

Prof. Dr. Canan Özgen
Dean, Graduate School of **Natural and Applied Sciences** ________________

Prof. Dr. Sinan Bilikmen
Head of Department, **Physics** ________________

Assoc. Prof. Dr. Akif Esendemir
Supervisor, **Physics Department, METU** ________________

Examining Committee Members:

Prof. Dr. Ramazan Aydın
Physics Department, Atılım University ________________

Assoc. Prof. Dr. Akif Esendemir
Physics Department, METU ________________

Prof. Dr. Halil Kırbıyık
Physics Department, METU ________________

Assoc. Prof. Dr. Enver Bulur
Physics Department, METU ________________

Assoc. Prof. Dr. Serhat Çakır
Physics Department, METU ________________

Date: ________________

I hereby declare that all information in this document has been obtained and presented in accordance with academic rules and ethical conduct. I also declare that, as required by these rules and conduct, I have fully cited and referenced all material and results that are not original to this work.

Name, Last Name: ÖZGE AMUTKAN

Signature :

ABSTRACT

SPACE RADIATION ENVIRONMENT AND RADIATION HARDNESS ASSURANCE TESTS OF ELECTRONIC COMPONENTS TO BE USED IN SPACE MISSIONS

Amutkan, Özge
Ph.D., Department of Physics
Supervisor : Assoc. Prof. Dr. Akif Esendemir

July 2010, 92 pages

Space radiation is significantly harmful to electronic components. The operating time, duration and orbit of the space mission are affected by the characteristic of the radiation environment. The aging and the performance of the electronic components are modified by radiation. The performance of the space systems such as electronic units, sensors, power and power subsystem units, batteries, payload equipments, communication units, remote sensing instruments, data handling units, externally located units, and propulsion subsystem units is determined by the properly functioning of various electronic systems. Such systems are highly sensitive against space radiation.

The space radiation can cause damage to electronic components or functional failure on the electronics. A precisely methodology is needed to ensure that space radiation is not a threat on the functionality and performance of the electronics during their operational lives. This methodology is called as "*Radiation Hardness Assurance*". In this thesis, the hardening of electronics against space radiation is discussed.

This thesis describes the space radiation environments, physical mechanisms, effects of space radiation, models of the space radiation environment, simulation of the Total Ionizing Dose, and "*Radiation Hardness Assurance*" which covers Total Ionizing Dose and Single Event Effects testing and analyzing of the electronics.

Keywords: space radiation environment, radiation hardness, total ionizing dose, single event effect, GEANT4.

ÖZ

UZAY RADYASYONU ORTAMI VE UZAY GÖREVLERİNDE KULLANILACAK ELEKTRONİK BİLEŞENLERİN RADYASYONA DAYANIKLILIĞININ DOĞRULANMASI TESTLERİ

Amutkan, Özge
Doktora, Fizik Bölümü
Tez Yöneticisi : Doç. Dr. Akif Esendemir

Temmuz 2010, 92 sayfa

Uzay radyasyonu elektronik bileşenlere önemli ölçüde zararlıdır. Uzay görevinin çalışma zamanı, süresi ve yörüngesi radyasyon ortamının karakteristiği ile etkilenir. Elektronik bileşenlerin ömrü ve performansı radyasyon ile değişir. Elektronik birimler, sensörler, güç ve güç alt birimleri, piller, yük taşıyıcı ekipmanları, iletişim birimleri, uzaktan algılama cihazları, veri taşıma birimleri, harici yer alan birimler ile itme altsistem birimleri gibi uzay sistemlerinin performansı çeşitli elektronik sistemlerin doğru işleyişi ile belirlenir. Bu sistemler uzay radyasyonuna karşı çok hassastır.

Uzay radyasyonu elektronik bileşenlerinde zarara ve fonksiyonel yetersizliğe neden olabilir. Uzay radyasyonunun, elektronik devrelerin işleyiş süreleri boyunca fonksiyonelliği ve performansında bir tehdit oluşturmadığına emin olunması için kesin bir yönteme ihtiyaç duyulur. Bu yönteme "*Radyasyona Dayanıklılık Doğrulaması*" adı verilir. Bu tez çalışmasında, uzay radyasyonuna karşı elektroniklerin dayanıklılığı tartışılmaktadır.

Bu tez, uzay radyasyon ortamları, fiziksel mekanizmalar, uzay radyasyonunun etkileri, uzay radyasyon ortamı modelleri, toplam iyonlaştırıcı dozun benzetişimi ve elektronik bileşenlerin toplam iyonlaştırıcı doz ve tek olay etkileri testi ve analizini içeren ”*Radyasyona Dayanıklılık Doğrulaması*”nı tanımlamaktadır.

Anahtar Kelimeler: Uzay radyasyon ortamı, radyasyona dayanıklılık, toplam iyonlaştırıcı doz, tek olay etkisi, GEANT4.

To my precious parents and my lovely siblings..
And also everybody who I love and who loves me..

ACKNOWLEDGMENTS

There are many people to thank for the help, guidance, and support provided to me during my study. First, I would like thank to my supervisor, Assoc. Prof. Dr. Akif Esendemir whose encouragement, supervision and support throughout my study.

I would also like to thank Dr. Behçet Alpat whom I had the honor to work for a year. He supported me in my experimental study and offered me to work in his laboratory with a nice working atmosphere. This thesis would not have been possible without his encouragement.

It is a pleasure to thank Assoc. Prof. Dr. Haluk Denizli who made this thesis possible with a moral support like a brother. I learned much during my discussions with him. This thesis would not have been possible without his support.

I would like to express my deepest gratitude to Assoc. Prof. Dr. Serhat Çakır for his excellent guidance, caring, and patience during my study.

It is a pleasure to thank Francesca Renzi for never tiring of my questions about the simulation program and her wonderful friendship. I enjoyed excellent working climate and discussions in the coffee breaks. I would also like to thank Diego Caraffini who was always willing to help and discuss.

I would like to thank Zati Ünal who helped for my simulation by giving Sarayköy Irradiation Plant settlement plan and source activity.

I am indebted to my colleagues, Nurcan Yanarcan, H. Cüneyt Eroğlu, Ercan Aydın for their help, friendship and smiling faces. I had really great time in the laboratory, especially during the period of writing reports.

I would like to thank my parents, my mother Safiya Amutkan and my father Turan Amutkan, for encouraging me since I was a little girl to pursue a career in science, and for their unconditional love and restless support. I would also like to thank my siblings, Damla and Çagla, for their patience during my study.

I would like to thank Emel Kilit, Rengin Peköz, and İpek Koçer Güler, who as good friends, were always willing to help and give their best suggestions not only in my research but also in my life. I would also like to thank Alper Aygar for his support during the period of writing this thesis.

In addition, I wish to thank all of my friends, it is not possible to mention all their names, that helped in this thesis.

Finally, I would like to thank Scientific and Technological Research Council of Turkey (TUBITAK) for the financial support during my study.

TABLE OF CONTENTS

LIST OF TABLES

TABLES

LIST OF FIGURES

FIGURES

CHAPTER 1

INTRODUCTION

The space radiation environment is complex as well as dynamic. Charged particles, electrons and protons are trapped in the Earth's magnetic field. The Earth is surrounded by belts of these particles, which is called as Van Allen Belts. In addition, the magnetosphere and outside of the Solar system is exposed to a flux of solar particles consisted of charged particles. Since the flux is a function of solar activity, it may increase sharply during the solar flares. Galactic cosmic rays that originate from outside of the Solar system consist of highly energetic heavy ions. These heavy ions can be hazardous on electronic systems. Space radiation is significantly harmful to electronic components. The operating time, duration and orbit of the space mission are affected by the characteristic of the radiation environment. The aging and the performance of the electronic components are modified by radiation. The performance of the space systems such as electronic units, sensors, power and power subsystem units, batteries, payload equipments, communication units, remote sensing instruments, data handling units, externally located units, and propulsion subsystem units is determined by the properly functioning of various electronic systems. Such systems are highly sensitive against space radiation.

Space systems require the usage of sophisticated electronic components with high performance and quality. These systems also require a high degree of perfection from starting to processing. However, electronic components of space systems are sensitive to radiation effects. Perfection of surface layers, interfaces and insulating layers can be ruined by ionization effects. In addition, the amount of charge can easily be deposited through the device by the passage of heavy ions or energetic protons.

The solution for making the electronic components less sensitive to space radiation damage is "*Radiation Hardness Assurance*". Radiation Hardness Assurance is composed of the following steps:

- The definition of the radiation environment or threat. This step provides the worst case radiation environment definition in a space mission. The mission parameters including orbit parameters such as inclination, period, perigee height, apogee height, and eccentricity, additionally launch time and mission duration are related to the definition of the radiation environment. Trapped particles, heavy ions from galactic cosmic rays, and particles from solar flares are relevant to the threat.

- The evaluation of the effects of space radiation on the electronic systems or components. The worst case definition of the environment provides sufficient information to consider the level of the damage on the electronic systems or components. The definition of the environmental effects is effective for the suitability of the electronic systems or components which is used in the space mission. Evaluation of the effects helps to obtain mission requirements in the early design stage.

- The evaluation of the usage of the electronic systems or components. This step includes radiation testing and determination of the performance of the device. If the device passes the test criterion, it is accepted as suitable for the mission. Otherwise, the system or component requires redesigning.

The purpose of this thesis is to describe the application of the hardness assurance to the particular case of electronic components which is used in a space mission. Chapter 2 describes the important terminology and units of fundamental physical concepts, radiation interaction with matter, and space radiation sources such as solar, cosmic and trapped particles in detail. The fundamental mechanisms of space radiation environmental effects are described in Chapter 3, and the impacts on electronic systems are discussed in terms of total ionizing dose damage and single event effects. In order to design a reliable space system, defining the orbital characteristics of the space system is also significant since it is required to reduce risks on space systems and to design low cost, high performance parts. In Chapter 4, space radiation models are explained for three main radiation sources. These models are *Trapped Radiation Belt Models, Solar Particle Event Models, and Galactic Cosmic Ray Models*. In addition, 500–700 km altitude is evaluated by the help of these models. Flux values and dose rates are also calculated for 500–700 km altitude mission. Dose rates will be used to define the lifetime of the component after radiation hardness assurance tests. Evaluation of the hazard helps to obtain mission requirements early in the design stage. Monte Carlo techniques can also be used to compute the interaction and transport of the particles on the system. In Chapter 5, a Monte Carlo method of simulation for total ionizing dose in a gamma irradiation plant is given in detail.The sensitivity of electronic devices to radiation is often very changeable and it is not possible to use the theory solely to predict the effect on a device of a given exposure to radiation. Actual irradiation tests can be evaluated as an integral part of a system. However, tests can sometimes be performed on each batch of parts. In Chapter 6, it is aimed to provide test standards, total ionizing testing, single event effect testing, and their test sources. In addition, a work which was submitted in Radiation Effects on Components and Systems as Paper Number 1112 for the radiation hardness assurance for irradiation of electronic components in air is given in Chapter 7.

CHAPTER 2

SPACE RADIATION ENVIRONMENT

2.1 Introduction

The natural space environment consists of electrons and protons trapped by Earth's magnetic field, protons and small amount of heavy nuclei produced by Solar events, and heavy nuclei, i.e. cosmic rays produced outside the Solar system. Some of these charged particles have sufficient energy to penetrate into space vehicles and can damage their electronics. These damages from charged particles significantly cause ionization. In this section, some important terminology and units of fundamental physical concepts, some forms of radiation interaction with matter, and space radiation sources such as solar, cosmic and trapped particles are given.

2.2 Basic Physical Concepts

2.2.1 Energy

Kinetic energy represents the energy of motion. When the particles have rest mass, the fundamental kinetic energy equation which is related to the mass and velocity can be given in the following:

$$E = (\gamma - 1)mc^2,\ \gamma = \left[1 - \left(\frac{v}{c}\right)^2\right]^{\frac{1}{2}} \ (\textit{Relativistic}) \tag{2.1}$$

$$E = \frac{1}{2}m_0v^2 \; (Non - Relativistic) \tag{2.2}$$

Where E is the kinetic energy of particle, m_0 is the particle rest mass, v is the velocity of particle, c is the speed of light.

Otherwise, for a photon which does not have a rest mass, the equivalent energy equation is given as:

$$E = h\nu \tag{2.3}$$

Where h is the Planck's constant (6.626068 x 10^{-34} m^2kg/s) and ν is the frequency of light.

Energy unit can be given in terms of the *Erg*, the *Joule* or *Electron Volt (eV)*. The Erg is the basic energy unit of CGS (Centimeter, Gram, Second) system and is represented in units of $g.cm^2/s^2$. However, the Joule is the basic energy unit of MKS (Meter, Kilogram, Second) system and is represented in terms of $kg.m^2/s^2$. The electron volt is a measure of energy gained by an electron through an electric potential difference of one volt. The relationship between the Erg, the Joule, and Electron Volt can be given as in the following:

$$1eV = 1.602x10^{-12}Ergs = 1.602x10^{-19}Joules \tag{2.4}$$

2.2.2 Radiation Dose

Radiation dose is a measure of deposited energy from an ionizing radiation per unit mass of some material. Since the energy deposition is dependent on the material, dose is represented as radiation absorbed dose. The dose units can be given in terms of radiation absorbed dose (*Rad*) or *Gray*. The Rad is the basic dose unit of CGS system and is represented in units of Erg/g. However, the Gray (Gy) is the basic dose unit of MKS system and is represented in terms of J/kg. The relationship between Gray and Rad can be shown as in the below:

$$1Gy = 1J/kg = 100Rads = 10^4 Ergs/g \tag{2.5}$$

2.2.3 Flux

In addition to the energy and dose, it is also necessary to express what the flux is. Flux is the amount of flows through a unit area per unit time. When the rate of energy transfers from the source through a unit area per steradian per second, it is called *Energy Flux* and is given in terms of J.m^{-2}s^{-1} in MKS system. However, if it is mentioned as particle flow, then the unit of flux is given as particle/m^{-2}s^{-1}. While speaking in terms of a time interval, this quantity is called *fleunce* and given as particle/m^{-2}.

2.2.4 Linear Energy Transfer

Apart from energy, dose, flux and fluence, another significant concept which is used to quantify the effects of ionizing radiation on electronic devices is linear energy transfer (LET). LET is a measure of the energy transferred per unit length of absorbing material. LET is defined as in the following:

$$LET = \frac{1}{\rho}\frac{dE}{dx} \tag{2.6}$$

where ρ is the density of material, E is the energy loss through the material, and x is the distance. LET is expressed in terms of MeV/(g/cm^2).

2.3 Interaction of Radiation with Matter

In the space radiation environment, there are many forms of radiation interacts with the material and may affect vital electronic components. Electrons, protons, gamma rays, alpha and beta particles are the primary concern of these interactions. Radiation interaction can be classified into two groups charged particle and photon (electromagnetic waves) interactions, separately. Charged particles directly ionize while passing through the material. However, uncharged particles and photons ionize indirectly or by secondary radiation. While a moving charged particle is passing through the material, it interacts with the atomic structure of the material since it has electrical field surrounding it. The particle is decelerated and the electrons in the atoms are accelerated by this interaction. If the accelerated electrons have enough energy to escape, this process is called ionization. However, uncharged moving particles does not have any electrical field, while they interact with material, they only lose energy and cause collisions or scattering. A photon can lose energy by the *Photoelectric Effect, Compton Scattering*, or *Pair Production* [1].

2.3.1 Charged Particle Interactions

Charged particles also interact with electron and nuclei of an atom. When a charged particle enters a material, first it interacts with the electrons and nuclei and then begins to lose its energy. This process ends with penetrating into the material. If the energy is emitted, then this procedure is called as *ionization* which is the production of electron-ion pairs in the material. The emitted energy can also result in the form of electromagnetic radiation which is called as *Bremsstrahlung* which is schematically shown in the Figure 2.1.

There are principally four possible interactions between a charged particle and an atom. If there is an inelastic collision between a charged particle and an electron, then velocity of the particle is significant. If the velocity is below the level in which Bremsstrahlung is important, electrons are led to excitation level and to ionization.

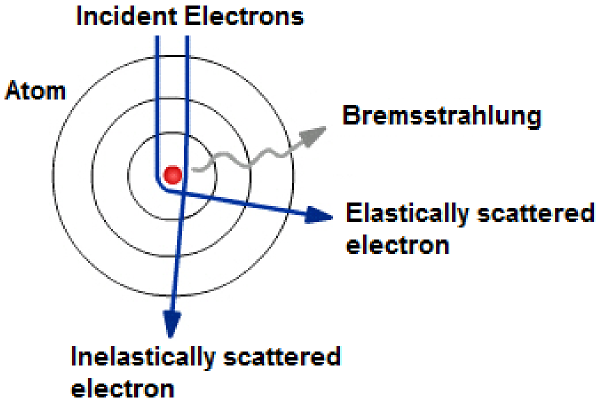

Figure 2.1: Schematic illustration of charge particle interactions [2].

If the interaction is elastic between a charged particle and an electron, this process results with a small amount of energy transfer. When there is an inelastic collision between a charged particle and a nucleus, charge particle may excite the nucleus or may radiate. If there is an elastic collision between a charged particle and a nucleus, there is neither excitation nor radiation. Since the particle does not have enough energy to penetrate the nucleus of the atom, it only loses energy. This process is called as *Rutherford scattering* [3] and is shown in Figure 2.2.

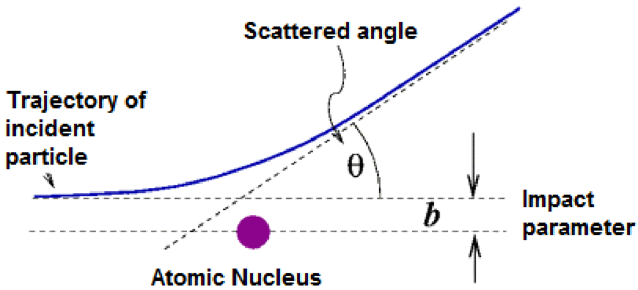

Figure 2.2: Schematic illustration of Rutherford scattering [4].

2.3.2 Photon Interactions

Apart from charged particles, electromagnetic waves interacts with matter, but these interactions are quite different from charged particle interactions. Electromagnetic waves have particle-like properties as discrete levels of energy, or quanta, called photons [6]. Photon is accepted as a particle whose rest mass is zero and charge is neutral. Gamma rays and X-rays are the two examples of high energy photons. A photon interacts on a matter in three types: *the Photoelectric Effect, Compton Scattering* and *Pair Production*. The energy of the photon determines the interaction which takes place on the matter. If the energy of the photon is less than 50 keV, then photoelectric effect may occur. If the energy of the photon is between 50 keV and 20 MeV, then Compton scattering may occur. If the energy of the photon is greater than 20 MeV, then pair production may occur [5].

2.3.2.1 Photo-Electric Effect

Photons have a characteristic energy determined by the frequency of the photon. If the energy of the photon is greater than the electron's binding energy, electron absorbs this energy and can be ejected from the atom. When the photon energy is absorbed, some of the energy discharges the electron from the atom and the rest contributes to the electron's kinetic energy as a free particle. This process which is shown in Figure 2.3 is called as Photoelectric Effect. The maximum kinetic energy of the ejected electron is given by:

$$E = h\nu - \phi_0 \tag{2.7}$$

Where ϕ_0=hν_0 is the threshold energy which is required to emit an electron from the atom and ν_0 is the threshold frequency of a given metal.

It is clearly understood from Equation 2.7 that the photoelectric effect occurs when the photon energy is greater than a threshold energy ($E = h\nu - h\nu_0$). In this case, the number of emitted electrons is proportional to the incident photon energy and has frequency $(\nu - \nu_0)$ [3, 8].

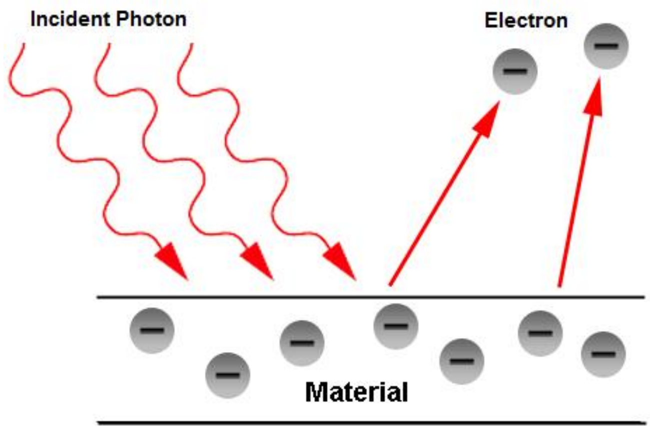

Figure 2.3: Schematic illustration of Photoelectric effect [7].

2.3.2.2 Compton Scattering

In the case of Photoelectric Effect, the photon has energy close to or greater than the binding energy of the electron. If the energy of the incident photon is much higher than the electron binding energy, the incident photon is deflected by the interaction with electron. The electron is ejected from its orbital position and can be considered as free. The interaction of the photon and this free electron is known as Compton scattering as shown in Figure 2.4. In the Compton Scattering phenomenon, the photon has an energy $E_1 = h\nu_1$ and momentum $p_1 = h\frac{\nu_1}{c} = \frac{h}{\lambda_1}$, where ν_1 is the frequency, λ_1 is the wavelength of the photon, and c is the speed of light.

If this photon collides with the electron, the electron takes the energy of the photon and recoils. The remaining energy of the scattered photon is given as $E_2 = h\nu_2$. It is obvious that E_2 must be less than E_1. As a result, the wavelength of the scattered photon must be longer than the wavelength of the incident photon. After the Compton Scattering, photon scatters with an angle θ by giving a portion of energy to the electron. The energy transfer can be explained by the following equation:

$$\lambda_2 - \lambda_1 = \frac{h}{mc}(1 - Cos\theta) \tag{2.8}$$

Where λ_1 and λ_2 are photon wavelengths before and after the collision, respectively. This quantity is derived from the conservation of energy and momentum.[8]

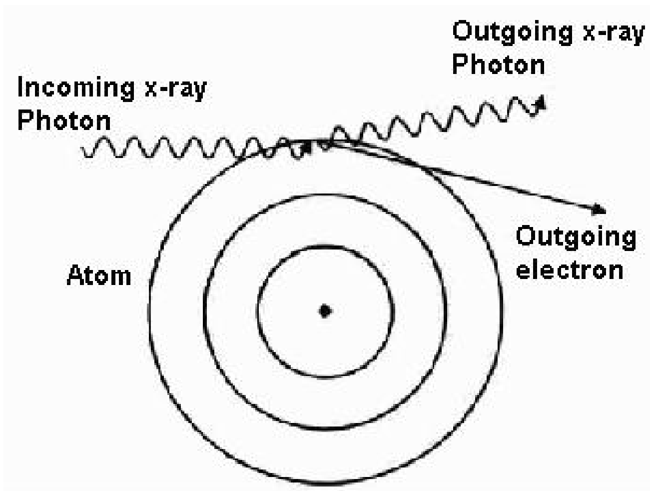

Figure 2.4: Schematic illustration of Compton scattering [9].

2.3.2.3 Pair Production

While a photon which has a sufficient energy is passing nearby a nucleus of the atom, it interacts with the nucleus, as a result an electron-positron (Positron is the anti-particle of the electron and has the same properties of an electron but positively charged) pair is formed [10]. This process is called as Pair Production which is illustrated in Figure 2.5 . For a pair production process to occur, a photon must have an energy which has to be at least 1.02 MeV, which is equal to the rest masses of two electrons [11].

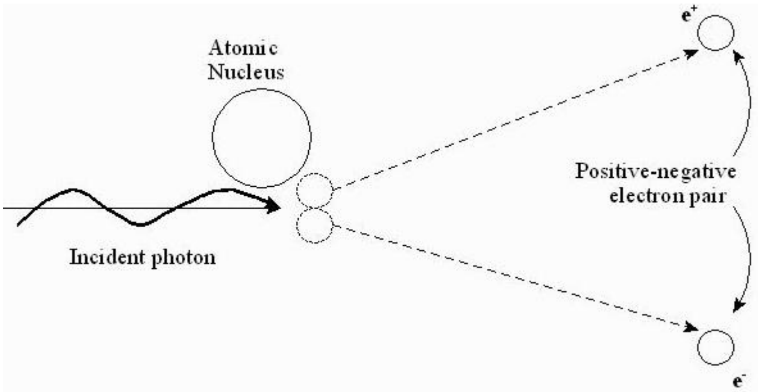

Figure 2.5: Schematic illustration of pair production process [12].

2.4 Sources of Space Radiation

The energy deposition in spacecraft materials, particularly electronic materials, can cause significant damage so that while planning a space mission, one must take into account ionizing radiation [13, 14]. Generally, ionizing radiation consists of both electromagnetic radiation such as UV-light, x-rays and γ-rays, and radiation caused by charged particles such as electrons (e^-), protons (p), alpha particles (α) and other heavier ions. The electromagnetic radiation which has a Solar origin is not a significant source of ionization in the interior of a space system, so it has a little effect on electronic systems. However, radiation caused by charged particles is a significant effect and causes energy deposition inside the space systems.

The space radiation environment can be classified into three main sources: *Solar particles*, *Geomagnetically trapped radiation near the Earth (Van Allen Belts)*, and *Galactic Cosmic Rays* [15]. Cosmic rays consist of energetic protons, electrons, alpha particles, and heavy ions of all the elements in the Periodic table. Particles trapped by the magnetosphere include protons, electrons, and heavy ions. Additionally, energetic protons, alpha particles, heavy ions, and electrons are the particles which are produced by solar eruptions.

Table 2.1: Energies of the particles in the space radiation environment.

Particle Type	**Maximum Energy**
Trapped Electrons	10s of MeV
Solar Protons & Heavy Ions	100s of MeV
Solar Protons	GeV
Solar Heavy Ions	GeV
Cosmic Rays	TeV

Particles and their energies are summarized in Table 2.1, [83]. In any space mission, space vehicles are under the influence of these particles depending on their orbits. It is important to understand the distribution of the sources and their effects while designing the space systems.

2.4.1 The Sun and The Solar Particles

The Sun is a star at the center of our Solar system and is the major source of space radiation environment. The Sun's chemical composition consists of mainly Hydrogen and Helium, while less than 2% consists of other elements such as iron, oxygen, carbon, neon and others [17]. Observation of the Sun shows that there are regions that appear darker than their surroundings on the surface of the Sun due to lower temperatures. These regions that are shown in Figure 2.6 are called *Sunspots*. Sunspots are caused by intense magnetic activity where convection is inhibited, forming areas of reduced surface temperature. Magnetic field also causes strong heating in the corona of the Sun that forms active regions which are the source of intense solar flares and coronal mass ejections.

As it is mentioned above, the Sun's magnetic field can change quite rapidly either locally or globally. The most rapid changes occur locally. However, global magnetic field changes occur in 11 year cycle. The number of sunspots is not constant. In every 11-year period, fewer and smaller sunspots and also solar flares which are the magnetic storms on the Sun, that appear to be very bright spot and gaseous surface eruption are observed on the surface of the Sun. This period is called *"Solar Mini-*

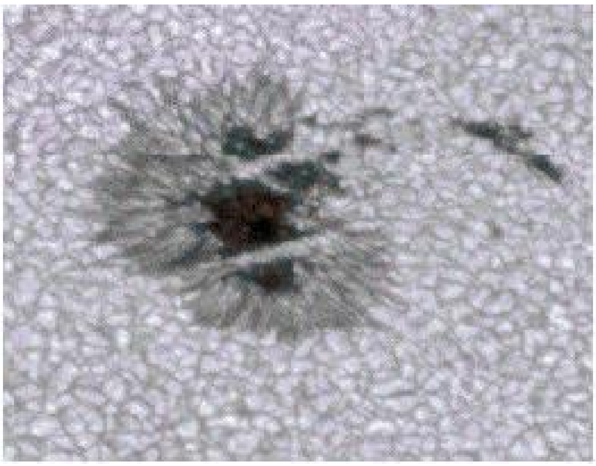

Figure 2.6: Sunspots are the regions of highly dense magnetic field in the Sun [18].

mum" and it takes approximately 4 years. However, when more and larger sunspots are observed, this period is called *"Solar Maximum"* and it takes approximately 7 years (see Figure 2.7).

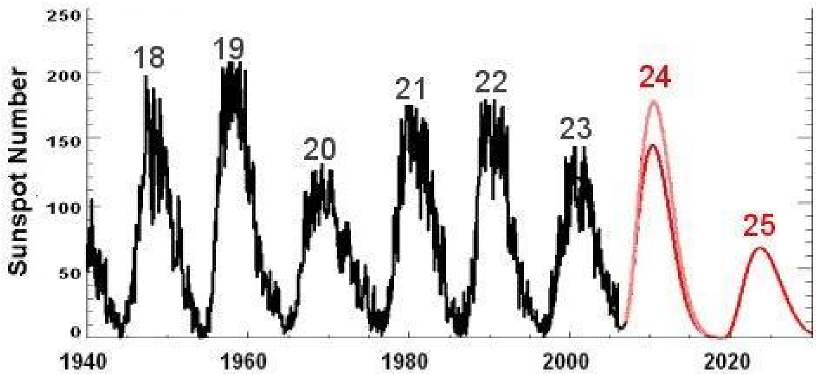

Figure 2.7: Past and expected future sunspot numbers for solar cycles.

The particles from solar events are important concern for spacecraft designers. The radiation created by the Sun can be classified into three types, electromagnetic waves, solar wind and solar flares [19, 50]. Electromagnetic radiation is non-ionizing and does not cause radiation damage. Ultraviolet and x−rays from the Sun can be hazardous in materials on the surface of the space system by ionization; however, those do not contribute total dose that are absorbed by the electronic components of the space system. Solar radiation affects the determination of the temperature distribution inside the space system. Apart from the Sun's activity period, another quantity that affects the level of the space radiation sources is *Solar Wind*. A solar wind is a continuous stream of ions that are given off by magnetic anomalies on the Sun. The flux of these ions is typically $10^8 - 10^9$ particles $cm^{-2}s^{-1}$ as measured outside the Earth's magnetosphere.

2.4.2 The Magnetosphere

The Magnetosphere is the region around the Earth where the influence of the earth's magnetic field decreases. This field plays a dominant role in determining the radiation environmental effects. Presence of the magnetosphere not only provides protection from cosmic rays and Solar particles, but also leads to the formation of regions where charged particles are trapped.

Solar wind particles can not easily penetrate into the Earth's magnetic field since they are decelerated and deflected by Earth's magnetic field. This interaction leads a formation between a magnetosphere and ambient medium which is called as *bow-shock* [21]. In contrast to the day-side magnetosphere which is compressed and confined by the solar wind, the Earth's magnetosphere has a tail which is called *magnetotail* in the night-side. Schematic illustration of the magnetosphere is shown in Figure 2.8.

When the solar wind interacts with the Earth's geomagnetic field, magnetotail stores its energy in the form of magnetic potential energy. This results causing a magnetic substorm and resulting in auroral activity into the upper atmosphere. This interaction can extend into the high altitudes causing the surfaces of spacecraft highly charged and sudden discharge by electrical arching on the surface of the spacecraft [23]. However, this is not a significant problem for low altitude space systems.

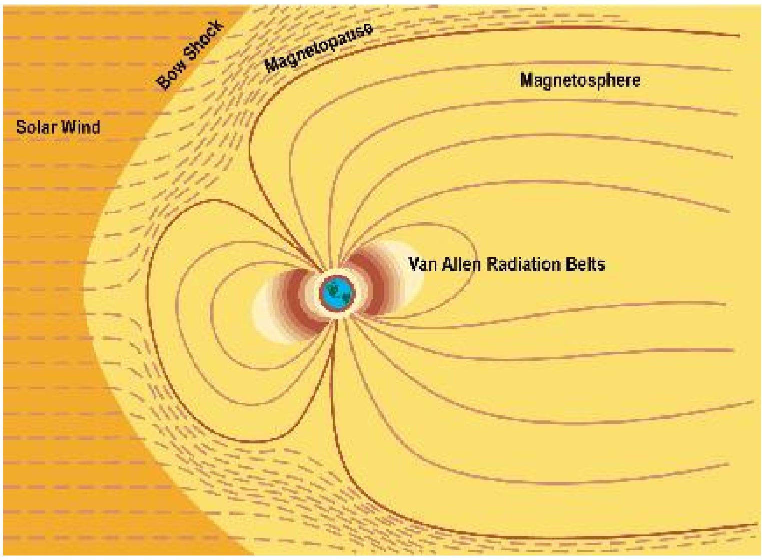

Figure 2.8: The Earth's magnetosphere is formed by the interaction of the solar wind and the Earth's magnetic field [22].

2.4.3 Geomagnetic Shielding

For charged particles to reach a spacecraft or the Earth's surface, they must penetrate the Earth's magnetic field. Penetrating ability of the particle is determined by its momentum divided by its charge, and this equation is referred to *Magnetic Rigidity, P*.

$$P = \frac{pc}{Ze} \tag{2.9}$$

Where p is the relativistic momentum which is expressed in units of eV/c, c is the velocity of light, e is the electron charge which is equal to $1.602x10^{-19}C$, and Z is the atomic number. Magnetic rigidity is expressed in units of GV.

2.4.4 Galactic Cosmic Rays

Galactic cosmic rays (GCR) are particles that originate outside the Solar system; however, a small amount of GCR originate from the Sun. Galactic cosmic rays are one of the most important radiation sources and thought to be uniform outside our Solar system. GCR consist mostly of protons (85%), alpha particles (14%), and less than 1% of electrons and gamma rays [24].

Galactic cosmic rays are affected by Earth's magnetic field. The Earth's magnetic field lines are parallel to the surface of the Earth at Equator and point toward at the poles of the Earth. At high altitudes where geosynchronous orbits are 35800 km), the Earth's magnetic field is weak enough that it can be considered as having negligible effect on GCRs [25]. However, when cosmic rays penetrate into the magnetosphere, low energetic particles can easily lose their energies.

Since GCRs have high energetic particles which can easily penetrate inside the space vehicle, these particles can be hazardous to space vehicle electronics. Additionally, GCRs have a high rate of energy deposition as measured by their LET rate [26]. The flux of cosmic radiation near the Earth decreases by the solar activity and reduces at the solar maximum [19]. When the solar activity is low, this means that the solar wind decreases. In this case, the GCR flux reaches its maximum level for solar minimum. On the contrary, when solar winds increases, in solar maximum, the GCR flux is at its lowest level [27].

2.4.5 Trapped Particles in Van Allen Belts

Earth's trapped radiation belts were discovered by Van Allen in 1958. Earth's geomagnetic field traps the charged particles coming from outer space and retains them for a long time [50, 28]. These trapped charged particles move helically around the geomagnetic field lines. There are basically two helical motions of the trapped particles between points near the north and the south poles: *sliding motion* along the geomagnetic field lines and *bouncing motion* along a line [29]. Additionally, there is also a *longitudinal drift* around the Earth. Electrons drift to the east, while protons drift to the west. Electrons and protons are the main particles of the trapped radiation. Trapped radiation depends on the intensity of the magnetic storms, and changes are short term and long term time dependent. While estimating radiation dose in space, both particle fluxes are averaged.

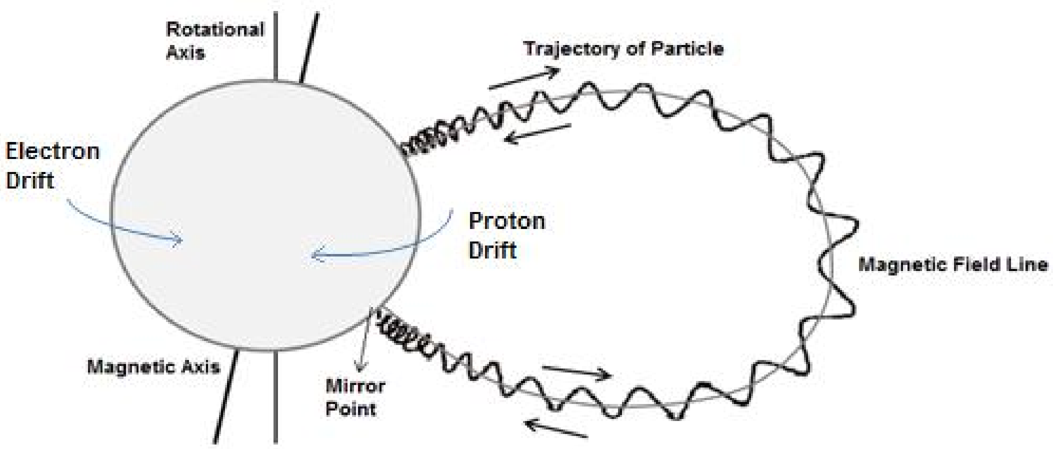

Figure 2.9: Charged particle motion in the Earth's magnetic field. During geomagnetic activity, energetic electrons are injected into the midnight meridian and they drift from midnight meridian towards the dawn meridian, while protons move along the magnetic field lines towards the dusk meridian [30].

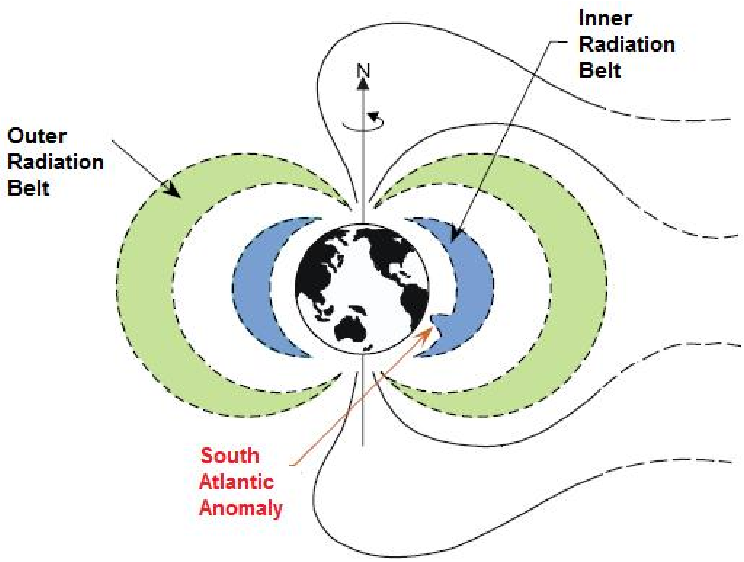

Figure 2.10: Illustration of trapped radiation belts around the Earth. South Atlantic Anomaly is the region where radiation belts reach their lowest altitude [31].

The magnetic field intensity increases at low altitudes. There is a region where the radiation belts reach their lowest altitude is called as *South Atlantic Anomaly* (SAA).

In this region shown in Figure 2.10, proton flux is particularly intense, therefore this region is an important source of radiation exposure for space systems traveling at low orbit inclination and low altitudes [32]. Additionally, electron distribution in Van Allen belts is also divided into two regions as compared in the Table 2.2 below [50, 33].

Table 2.2: Comparison of two zones belonging to Van Allen belts.(R_E is the Earth mean radius which is equal to 6371 km.)

Inner Zone
Lies in the range of 1.2 to $2.5R_E$
Proton flux is dominant
Electron energies are smaller than 5 MeV
Electron and Proton fluxes peak at $1.5R_E$ to $2R_E$
Outer Zone
Lies in the range of 3 to $11R_E$
Electron flux is 10 times higher than inner zone
Electron energies are around 7 MeV
Electron peaks at $5R_E$

CHAPTER 3

SPACE RADIATION EFFECTS ON SPACE SYSTEMS

3.1 Introduction

For every space systems to operate in the space environment, it is necessary to define the environmental effects on the systems before launching and it is also important to define the radiation levels within the space systems. In this chapter, the fundamental mechanisms of space radiation environmental effects are described, and the practical impacts on electronic systems is discussed in terms of total ionizing dose damage and single event effects (SEEs).

3.2 Total Ionizing Dose Effects

The total ionizing dose (TID) effect, caused by trapped protons and electrons contained in radiation belts and protons emitted by solar flares, can result in device failure or biological damage to astronauts in space systems. In low altitudes, the main dose source is caused by electrons and protons, while in high altitudes in other words geostationary earth orbit, the main dose source is from electrons and solar protons. TID is measured in terms of absorbed dose (See Section 2.2.2).

The total ionizing dose depends on altitude, inclination, and time. TID is computed according to the exact location of the space system. Total dose levels are calculated for all parts, taking into account spacecraft shielding. In order to evaluate TID, one needs to use the *dose depth curve* which notifies the dose received through a shield thickness. Shield thickness is often identified as being a hollow aluminum sphere. Dose depth curve is used to specify the mission requirements for radiation assurance [34].

3.2.1 Dose Levels for Low Earth Orbit

A low Earth orbit (LEO) is an orbit where extends between 160–2000 km above the Earth's surface [35, 36]. The environment in LEO is fairly harmless while the space system is passing near the high latitudes (poles) in outer electron radiation belt and while the space system is passing from the South Atlantic where the trapped particles have high levels [37].

A LEO space system receive 0.1 kRads/year (1 Gy/year) dose rates for a mission. For a typical 3-5 year mission, the total dose is ¡ 0.5 kRads [38]. While a LEO orbiting space system is in around a very low equatorial orbit, it is exposed to less radiation. Moreover, while a space system is in a low orbit but has less than 45^0 inclination, SAA affects the space system. Additionally, while a space system is in a polar orbit but has greater than 55^0 inclination, space system is subjected to both SAA and in poles. Finally, if a space system is placed at an altitude higher than 1400 km, it is affected by high radiation dose due to trapped particles in Van Allen belts [37].

3.2.2 Dose Levels for Geostationary Earth Orbit

A geostationary orbit (GEO) is an orbit which lies in the plane of Earth's equator and is at an altitude of 36000 km. A space system in GEO is exposed to outer radiation belts, solar flares and cosmic rays. In GEO, a space system receive approximately 10 kRads/year (0.1 kGy/year) dose rate. For a typical 10 year mission, the total dose is 100 kRad [38].

3.2.3 Dose Levels for Medium Earth Orbit

Medium Earth Orbit (MEO) is an orbit which extends from 2000 to 36000 km above the Earth surface. Since a space system is mostly within the Van Allen belts in MEO, it is harshly exposed to radiation. The environment in MEO is highly affected by the solar cycle effects and the dose rate is in the order of 100 kRads/year (1 kGy/year) [38].

3.2.4 Physical Mechanism of Total Ionizing Dose

When energized particles pass through the material, they can cause ionization. Total ionizing dose refers to the amount of energy which is created and deposited in a material by ionization. Ionization produces electron-hole pairs within insulators and semiconductors. When an electron-hole pair is produced, the electron in the valance band is excited to the conduction band, resulting a hole behind in the valance band. Both the conduction band electrons and the valance band holes contribute to the electrical conductivity. While the created electrons can drift, holes can diffuse in the material until creating recombination or trapping. Insulators contain trapping centers where the radiation-induced charge can rest for long times. These trapped charges produce voltage offsets or shifts in electrical operating characteristics of the device by generating internal space-charge electric fields resulting failure in the device [39].

Another effect on total dose degradation is *biasing*. Biasing is a method to prove predetermined voltages and/or currents of an electronic circuit for setting the operating point properly. The operating point of the device is a point where the direct current (DC), collector-emitter voltage V_{CE} and collector current I_c without input signal is applied [40].

When a bias potential is applied, there will be an electric potential across the gate oxide into Silicon oxide. If the gate bias is sufficiently large and positive, it will cause

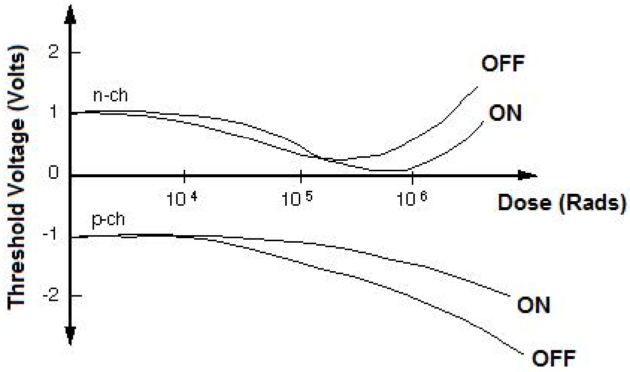

Figure 3.1: Threshold voltage shift versus dose for n-channel and p-channel transistors.

the holes in order to be transported to the silicon-silicon dioxide interface and cause trapping. In the opposite case, if the gate bias is negative, it will cause the holes to be transported to the gates and cause recombination of electrons [41].

Threshold voltage is the minimum voltage that is required to make the transistor on. The threshold voltage is changed by the trapped holes at the silicon oxide interface. Radiation induced charging generates additional space-charge fields at silicon surface. These additional induced fields cause shifts in the threshold voltage on the device. Figure 3.1 shows the threshold shifts because of recombination in the oxide [41].

3.3 Single Event Effects

A *Single Event Effect* (SEE) is caused by striking a single, energetic particle deposited along the track of a microelectric device. Single event can be classified into three forms: *Single event upset, Single event latchup, Single event burnout.*

3.3.1 Physical Mechanism of Single Event Effects

When a heavy ion or a proton pass through a medium, it goes straight a line. During its penetrating a device, it deposits energy along the track. Depending on the LET

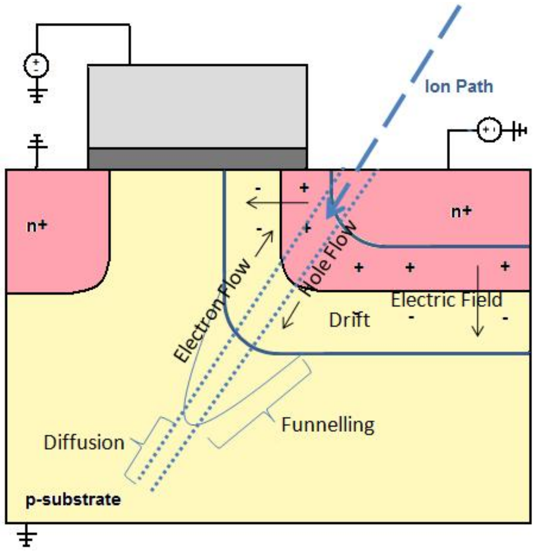

Figure 3.2: Ion track due to single ionizing particle penetration [42].

of the particle, energy is deposited in a path-length, generating electron-hole pairs. These charges quickly migrate under the influence of electric fields within the device. While some of the deposited charges recombines, some of them are trapped.

3.3.1.1 Single Event Upset (SEU)

Single event upset (SEU) is defined as a radiation induced error in microelectronic circuits. While charged particles are passing through the medium, they lose their energy by ionizing the medium, leaving behind a wake of electron-hole pairs [43]. SEUs are transient soft errors, and they are non-destructive. Device functionality can return to its original behavior, after resetting or rewriting. SEU can affect analog, digital and optical components, and their surrounding circuits.

3.3.1.2 Single Event Latchup (SEL)

Latchup is a term which is used to describe a particular type of short circuit in the integrated circuit. SEL mostly originates from heavy ions and protons in sensitive devices [45, 46]. While a heavy ion or a high energy proton is passing through the one of the two inner transistor junctions can turn on the semiconductor device, then it stays shorted until the device is power cycled [47]. By the reason of a single event induced current state, single event latchup (SEL) leads to losses in the functionality of the device [44]. Unlike single event upset, SELs are hard errors, and they are destructive. Device functionality can return its normal behavior by setting a power Off-On or strobing. SEL strongly depends on temperature. For this reason, it is important to strobe power while SEL occurs. Otherwise, excessive heating may cause catastrophic failure in the device [48, 49].

3.3.1.3 Single Event Burnout (SEB)

High current state in a power transistor causes device failure which is called as single event burnout (SEB). If sufficient energy is available to destroy the device, SEB occurs only in power devices at higher voltages. SEBs are considerably hard errors, and cause permanent failure in the device [50].

3.3.2 Quantification of the Electronic Device to Single Event Effects

High energy Galactic Cosmic Rays or Solar heavy ions can be simulated by using low energy ions in particle accelerators. In order to quantify the susceptibility of an electronic device to single event effects, there are two parameters: *Linear energy transfer threshold* (LET_{th}) and the device SEU-sensitive *cross section*. LET_{th} is defined as the minimum LET to cause single event effect at a particle fluence of $10^7 ions/cm^2$ [51]. The importance of LET_{th} is that the energy deposition can be triggered the effect, when LET is greater than the threshold. In order to be immune to single event effects of a device, LET_{th} must be greater than $100 MeV.cm^2/mg$ which is defined for iron ion. Proton sensitivity is implied by low LET_{th}. For analyzing SEU rates and effects as a function of immunity Table3.1 can be used [51]:

Apart from threshold LET, the second parameter to quantify the susceptibility of an electronic device is SEU-sensitive *cross section*. Cross section is a quantity that rep-

Table 3.1: Generic linear energy transfer threshold and corresponding space environment to be assessed.

Device LET_{th}	**Environment to be Assessed**
$LET_{th} < 10 MeV.cm^2/mg$	Cosmic Rays, Trapped Protons, Solar Flares
$LET_{th} = 10 - 100 MeV.cm^2/mg$	Cosmic Rays
$LET_{th} > 100 MeV.cm^2/mg$	No analysis required

resents the probability to hit a surface area of the component of an ion. Cross section is given in the units of cm^2. Additionally, the incident angle of the particle is also an important parameter. *Incident angle* is the angle that upsets occur for a given particle LET. This angle is also known as *critical angle* (θ_c). If the incident angle diverts from normal incidence, the path length will increase. For heavy ions, the angle of incidence can be varied to increase the effective LET (LET_{eff}). The incident angle can be given as a function of effective LET and the LET value for the normal incidence by the following:

$$Cos(\theta_c) = LET/LET_{eff} \tag{3.1}$$

Incident angle must be in the range of θ_c and $\pi/2$, so that particles can produce upsets. It is important to mention that LET_{eff} is always smaller than LET_{th}. There are two possible cases in order to produce upsets. If LET is greater than LET_{eff}, this means that particles that come by all incident angels are capable of producing upsets. On the contrary, if LET is smaller than LET_{eff}, it is required to produce upsets that there must be an critical angle [48, 49].

3.3.2.1 Upset Rate Calculation

There are three steps in order to calculate the upset rates. First step is to measure the cross section versus LET by using a beam test method. The device cross section is expressed as the ratio of the number of upsets to the particle fluence.

The second step which is the most difficult parameter to define is to determine the sensitive device volume. It is mentioned before that in order to produce an upset, an ion must deposit a charge which is greater than the critical charge with in a sensitive volume. The device physical volume is actually is greater than the sensitive device volume. The third step is to determine the device error rate. Upset rate can be described in terms of $errors/bit.day$. Hardened devices are of the order of $10^{-8} errors/bit.day$ error rates.

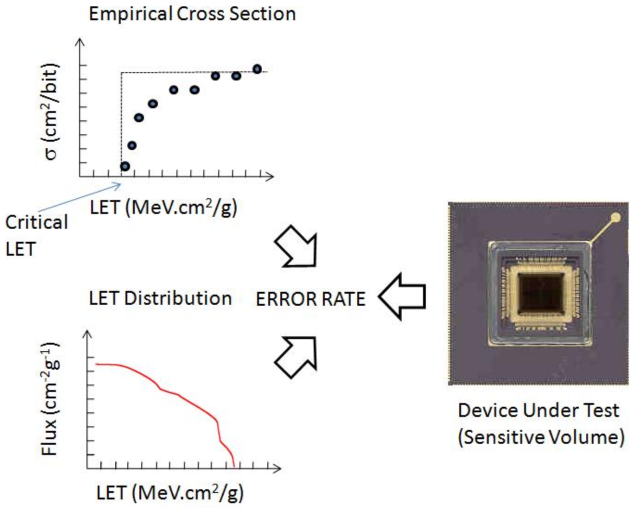

Figure 3.3: Illustration of the three main factors used to determine the Single Event Effects error rate calculations [52].

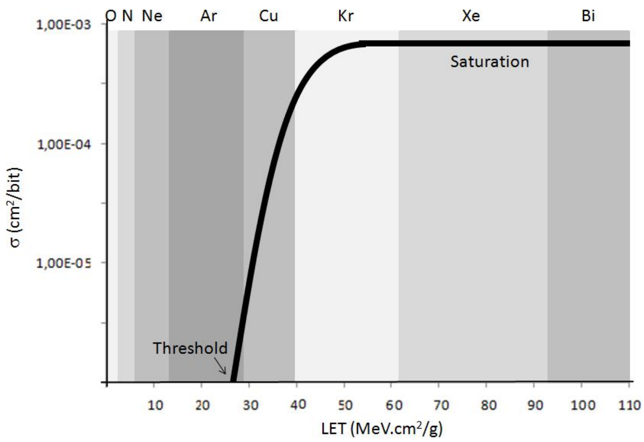

Figure 3.4: Cross Section versus LET curve in terms of ions used in testing [53].

In the Figure 3.4, there is a minimum LET value which is called the threshold LET. Above the threshold LET, when LET increases, cross section value also increases up to a specific value where the increment does not affect upset rate. After this value, all particles contribute equally to the effect of upset rate.

CHAPTER 4

MODELS FOR DEFINING THE SPACE RADIATION

4.1 Introduction

Trapped particles, heavy ions from galactic cosmic rays, and particles from solar flares are the main sources of the space radiation environment. In order to design a reliable space system, defining the orbital characteristics of the space system is also significant since it is required to reduce risks on space systems and to design low cost, high performance parts. In this chapter, space radiation models are explained for the three main radiation sources. These models are *Trapped Radiation Belt Models, Solar Particle Event Models, and Galactic Cosmic Ray Models*. In addition, an orbit in 500–700 km altitude will be evaluated by the help of these models. Evaluation of the hazard helps to obtain mission requirements early in the design stage.

4.2 Trapped Radiation Belt Models

4.2.1 The NASA Models: AP–8 and AE–8

There are some different ways to model the trapped radiation environment. The best known and widely used trapped radiation belt models are AE8 and AP8 models for electrons [54] and protons [55], respectively. These models developed at Aerospace Corporation for the NSSDC at NASA/GSFC were based on satellites data taken in the 1960s and early 1970s. In AP8 model for protons, proton energies vary from 0,1 to 400 MeV. Whereas, in AE8 model for electrons, electron energies vary from 0,04 to 7

MeV. After defining an orbit, generating a trajectory, and transforming it to geomagnetic coordinates, these models give omnidirectional fluxes to the user. Despite the fact that AE8 and AP8 models are widely used, they have some disadvantages. Even though, the models have separate versions for solar minimum and solar maximum, temporal behavior of fluxes are not described. Additionally, flux directions are not explicitly defined. Since particle fluxes sharply rise on the inner edge of the radiation belts, in other words at low altitudes, large errors may occur in fluxes in computing. As a result, this can be a problem during the geomagnetic field shifting, since the conditions are not the same while the data acquired. In order to avoid to get large flux error at low altitudes, AE8 and AP8 models must be used with a compatible geomagnetic field models shown in Table 4.1. While computing fluxes by using another geomagnetic field models can give large flux errors at low altitudes [56]. Even though using the models together with the geomagnetic field models can reduce the errors in fluxes, these models do not give the features of some locations e.g. South Atlantic Anomaly, or does not compute particle fluxes which are expected for today missions. Therefore, the average results obtained from the models are given.

Table 4.1: Standard field models to be used with radiation belt models.

Radiation Belt Model	**Geomagnetic Field Model**
AE8–MIN	Jersen–Cain 1960
AP8–MIN	Jersen–Cain 1960
AE8–MAX	Jersen–Cain 1960
AP8–MAX	GSFC 12/66 extrapolated to 1970

The Figure 4.1 shows the predicted distributions of proton and electron with energies above 10 MeV and 1 MeV, respectively, by using NASA AP8 MAX and AE8 MAX models [54]. Energetic protons whose energy is greater than 10 MeV is confined in the Earth's magnetic field up to 20000 km. In addition, high energetic electron distribution is characterized by two zones below altitudes of one Earth radii and above two Earth radius. Between these regions, there is a region of low intensities called as *slot*. Electron energy changes in inner and outer belts, and in the slot region depending on the location and extension. Higher energetic electron population is confined to

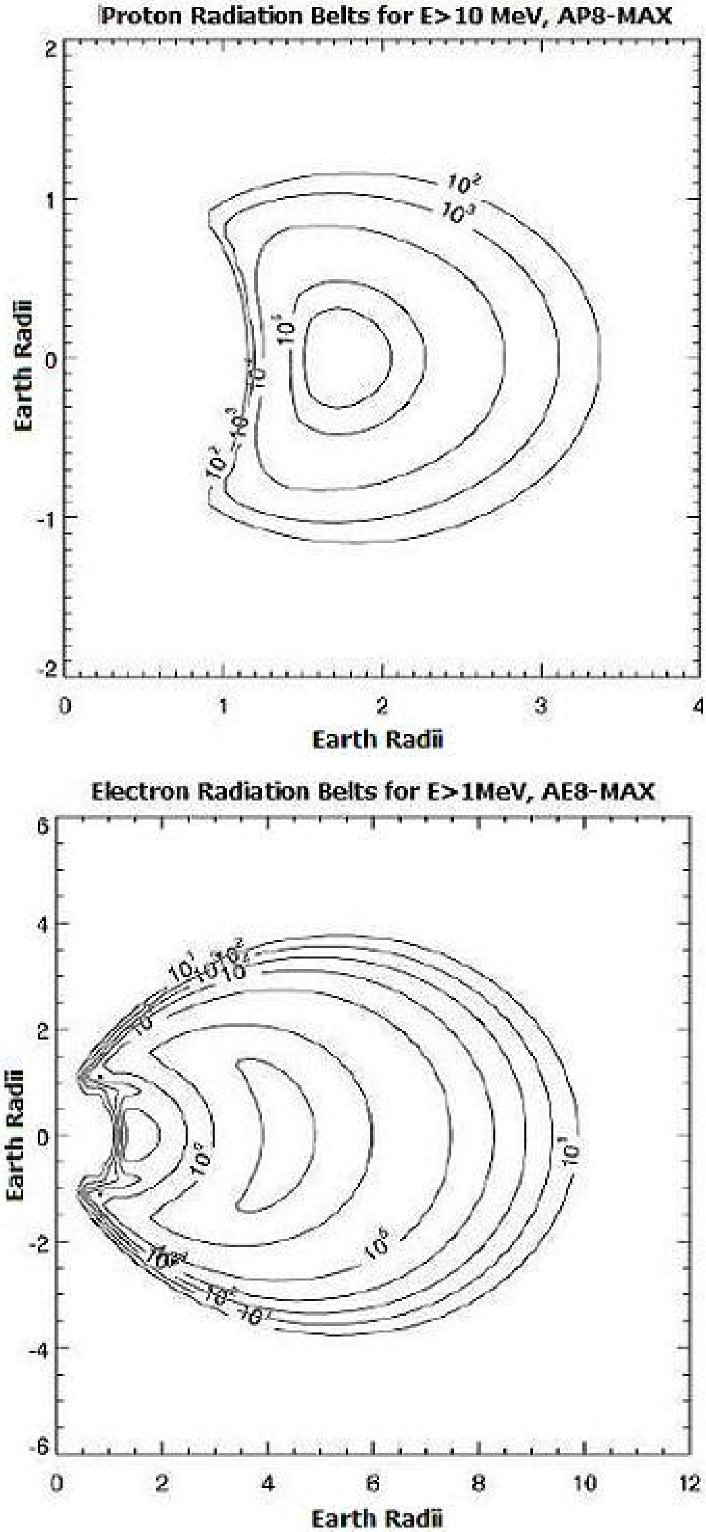

Figure 4.1: Contour plots of electron and proton radiation belts of the Earth [54].

inner belt, while lower energetic electron population is confined to outer belt to the altitudes beyond geosynchronous orbit.

4.2.2 Currently Available Other Trapped Radiation Models

Except from AE8 and AP8 models, there are totally seven available models used for the trapped environment. These models are briefly given in Table 4.2 for proton and electron, separately. Proton models are PSB97 [57] which was developed by Belgian Institute for Space Aeronomy in 1997, Low Altitude Trapped Radiation Model (LATRM) [58] developed by The Boeing Co. in 1998, Trapped Proton Model (TPM–1) [59] developed by S.L. Huston from The Boeing Co. in 2002 and the Combined Release and Radiation Effects Satellite Proton Model (CRRESPRO) [60] developed by the Air Force Research Laboratory in 1993.

In addition, electron models are Combined Release and Radiation Effects Satellite Electron Model (CRRESELE) [61] developed by the Air Force Research Laboratory in 1992, Flux Model for Internal Charging (FLUMIC) [62] developed by DERA in 1999, and the Particle ONERA-LANL Electron (POLE) model [63] developed by LANL/ONERA in 2003.

4.3 Solar Particle Event Models

4.3.1 Solar Proton Models

Energetic protons which have large fluxes are produced by the Sun during energetic events on the Sun. Since solar particle events are undeterminable and have large variations in their magnitudes, duration and spectral characteristics, they have to be modeled statistically. If spacecraft spends an important amount of time in the interplanetary environment, one needs to estimate these uncertainties. Three proton event models are available for predicting long term proton fluences: *the King model* [65],

Table 4.2: Currently available trapped proton and electron models [64]

Proton Models	Energy Range	Features
CRRESPRO	Omnidirectional, differential or integral protons in 1–100 MeV range	Valid for solar maximum, Magnetic storm quiet or active, Internal or external field models
PSB97	Directional, differential or integral protons in 18.5–500 MeV range	Valid for solar minimum, Internal field model
LATRM	Omnidirectional, integral protons in >16, >30, >80 MeV range	True solar cycle variation, Internal field model, Secular variation of Earth's magnetic field
TPM–1	Omnidirectional, differential protons in 1.5–81.3 MeV range	Low altitude solar cycle variation, Internal field model, Secular variation of Earth's magnetic field, Magnetic storm quiet or active, 1 month time resolution
Electron Models	**Energy Range**	**Features**
CRRESELE	Omnidirectional, differential or integral electrons in 0.5–6.6 MeV range	Valid for solar maximum, Magnetic storm quiet or active, Internal and external field models, Outer electron belt only
FLUMIC	Directional, integral electrons in >0.2 to >5.9 MeV range	Worst case 1 day fluence, Solar cycle variation, Internal and external field models
POLE	Omnidirectional, integral electrons in 0.03–2.5 MeV range	Mean, worst case and best case models, solar cycle variation, 1 year time resolution

the JPL model [66], and *the ESP models* [67, 68] for total fluence and worst event fluence.

The King solar proton model was used for a long time in order to predict integrated solar proton fluences. The data used in the King model was entirely obtained during the active period of solar cycle 20 in 1966–1972. The King model was developed by National Space Science Data Center (NSSDC) in the USA [69]. The JPL model was constructed using data obtained from solar cycles 20, 21 and part of 22. The JPL model comprises daily average fluxes >1, >4, >10, >30, >60 MeV. Although, the King and JPL models are useful while predicting event fluence for long term degradation, they have limitations in proton energy range. In addition, the ESP model developed in NASA Space Environment and Effects (SEE) extends energy range up to 300 MeV. However, the standard solar proton models used for engineering consideration of time integrated effects are the JPL and ESP models.

4.3.2 Solar Heavy Ion Model

The standard solar heavy ion model is the Cosmic Ray Effects on Micro-Electronics 1996 Revision (CREME96). CREME96 model allows to create of energy spectrum, evaluation of radiation effects on electronics in spacecraft in different altitudes and estimate of LET spectrum for the worst week, worst day, and peak 5 minutes. [70]

4.4 Galactic Cosmic Rays Environment Models

Cosmic Ray environment models were developed in US Naval Research Laboratory [71] with the name of Cosmic Ray Effects on Micro-Electronics (CREME). CREME provides a complete set of Cosmic Ray and Solar event ion LET and energy spectra which includes attitude of geomagnetic and material shielding. CREME replaced by CREME96 [70]. The differences between CREME and CREME96 are that CREME96 includes the Cosmic ray environment and its solar cycle modulation, and also has an improved geomagnetic and material shielding calculation and has more realistic Solar energetic particle event ion environments [34]. CREME96 also provides the highest cosmic ray fluxes which occur in solar minimum since cosmic ray fluxes are anti-correlated with solar activity. In addition, in CREME96, it is possible to define the mission galactic cosmic ray environment ions from $Z = 1$ to $Z = 92$. As a result, CREME96 is the standard model used to define cosmic ray environment assessment.

4.5 Evaluation of Environment for 500–700 km Altitude

4.5.1 A Toolkit For Space Environment

In order to evaluate space environment and radiation effects in the 500-700 km altitude, OMERE toolkit developed by TRAD was used. The radiation constraints can be calculated by using this free usage software for a satellite in orbit. Charged particles environment (electrons, protons and heavy ions) can be computed by using orbit parameters or any specific trajectory file. The radiation effects on electronics and single event effects can be estimated by principally defining the environment. The software includes most of the standard models [72].

OMERE software which is developed in C++ allows the user to calculate the particle fluxes encountered by a satellite throughout the mission. It uses standard international trapped particle models, AE8 and AP8 with different magnetic field models such as IGRF, Jensen Cain, GSFC. For solar particles, OMERE is divided into two parts: solar protons and peak fluxes for Single event effects calculation. For Cosmic rays, OMERE uses CREME96. In addition, in OMERE, LET spectrum for solar particle and cosmic rays can be included.

4.5.2 Prediction of the Environment

The prediction of 500-700 km in different altitudes and inclinations was done to understand the environment in these ranges. Additionally, dose rates were calculated. Trapped electron and proton models for 500-700 km altitudes and different inclinations (28.5^0, 60^0 and 90^0) are presented in Table A.1 and A.2. Figure 4.2 presents the averaged orbit integrated fluxes for electrons as a function of energy, parametrically for orbital altitudes 500 km, 600 km, 700 km for 60^0 inclination. In addition, Figure 4.3 presents comparable data for electrons, parametrically for orbital inclinations 28.5^0, 60^0 and 90^0 for 500 km circular orbit altitude for the year 2010.

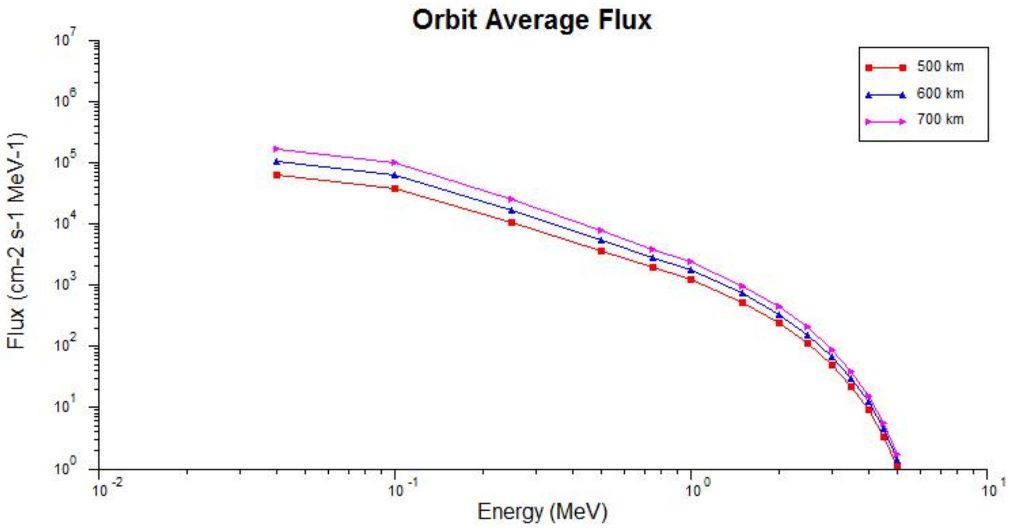

Figure 4.2: Averaged integral trapped electron flux in 500 km, 600 km and 700 km altitude, respectively, with the inclination 60^0 by using AE8-MIN model.

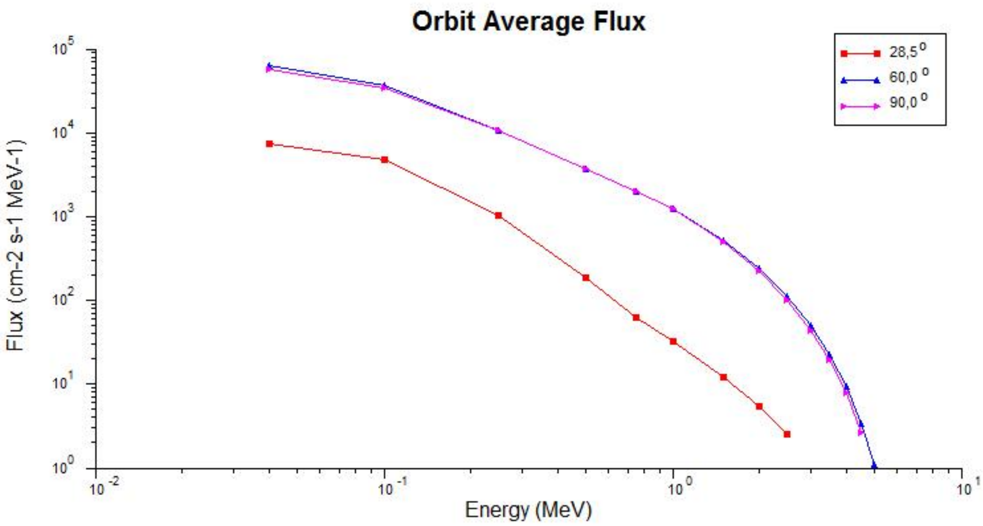

Figure 4.3: Averaged integral trapped electron flux with 28.5^0, 60^0 and 90^0 inclination, respectively, at 500 km altitude by using AE8-MIN model.

Figure 4.4 presents the averaged orbit integrated fluxes for protons as a function of energy, parametrically for orbital altitudes 500 km, 600 km, 700 km for 60^0 inclination. In addition, Figure 4.5 gives the integral comparable proton spectra for a circular 500 km altitude for inclinations 28.5^0, 60^0 and 90^0 in solar minimum for the year 2010.

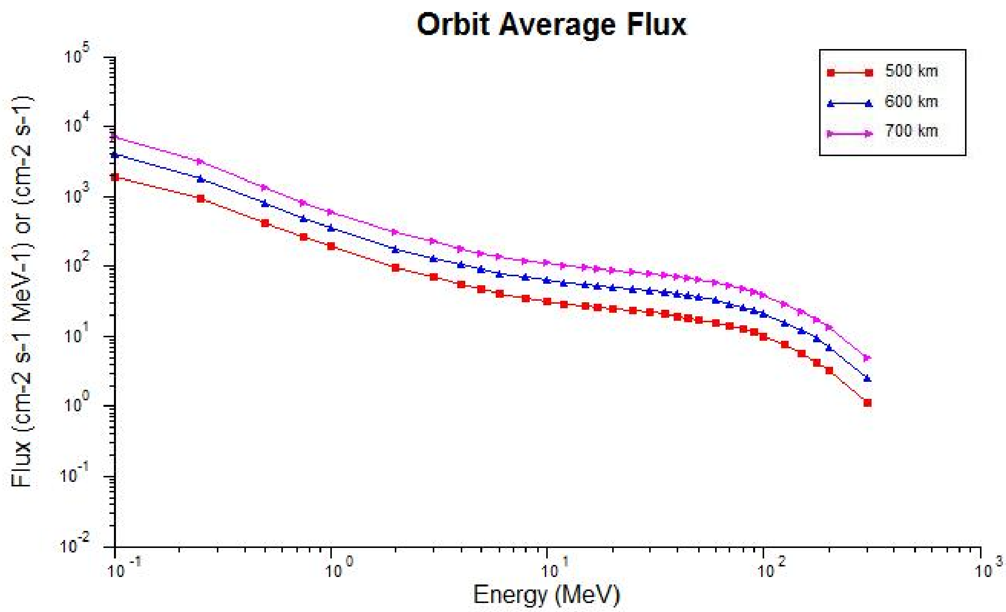

Figure 4.4: Averaged integral trapped proton flux in 500 km, 600 km and 700 km altitude, respectively, with the inclination 60^0 by using AP8-MIN model.

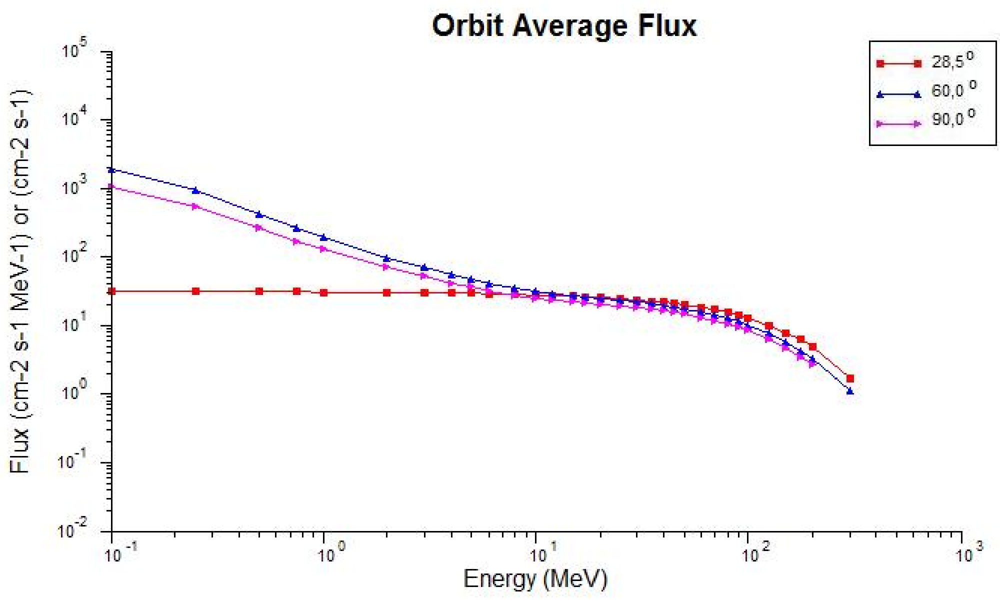

Figure 4.5: Averaged integral trapped proton flux with 28.5^0, 60^0 and 90^0 inclination, respectively, at 500 km altitude by using AP8-MIN model.

The trapped particle population in 500–700 km altitude is influenced by secular changes in the Earth's geomagnetic field. The location of the center of the geomagnetic dipole field drifts away from the center of the Earth. Figure 4.6 represents that the separation of the dipole center from the Earth's center and the inclination of the magnetic axis with respect to the rotation axis creates a local depression in 500–700 km altitude.

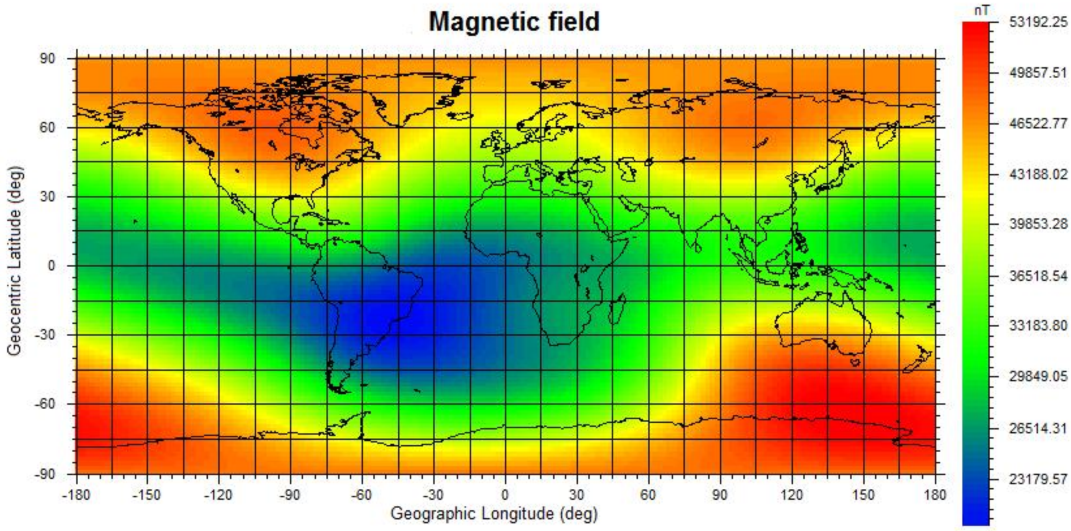

Figure 4.6: World map of the integral flux at 500 km altitude.

Figures 4.4 and 4.2 show that flux increases as the altitude increases. However, at 500 km altitude, 28.5^0 inclination has the lowest flux value. Low altitude and low inclination are acceptable for the space mission which is placed in the 500-700 km altitude range with the inclinations 28.5^0, 60^0 and 90^0.

In addition to the trapped charged particles in Van Allen radiation belts (electrons and protons), the space vehicle experiences radiation threats from solar particles. Proton fluence from solar particle events integrated over mission durations (1 year solar minimum and 4 years solar maximum) is derived using the ESP model. In the Figure 4.7 and in the Figure 4.8, the flux of solar particles is shown for 500 km altitude circular orbit and 60^0 inclination.

Since the trapped particle population depends on the magnetic field, the lowest altitude radiation environment peaks in South Atlantic Anomaly (SAA). Electron concentrations observed between 45 degrees and 85 degrees latitude in both the northern and southern hemispheres are higher. In 500 km–700 km altitudes, for low inclinations electron concentrations are relatively low.

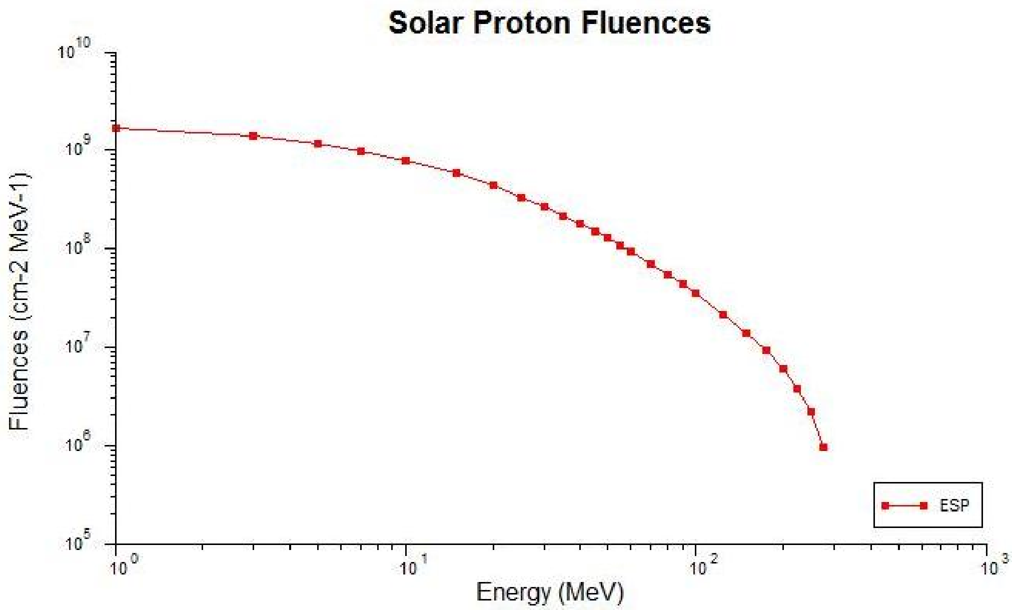

Figure 4.7: Integral fluence versus energy spectra for protons for a five year mission whose one year is in solar minimum and four years are in solar maximum at the 80 % confidence level.

For single event effects analysis, the solar flare proton flux is required. Reasonable estimates of the proton flux can be obtained from the CREME96 model on average over the worst day of the solar cycle.

The Galactic cosmic rays are also affected by the Earth's magnetic field. The Earth's magnetic field provides a significant shielding in 500 km–700 km altitude. While a space vehicle is passing through in these altitudes, it receives a large amount of cosmic rays near the poles. However, a space vehicle receives a small amount of galactic cosmic rays while passing through the equator. This feature is given in Figure 4.9.

The Galactic cosmic rays flux in 500–700 km altitude is modulated by the solar ac-

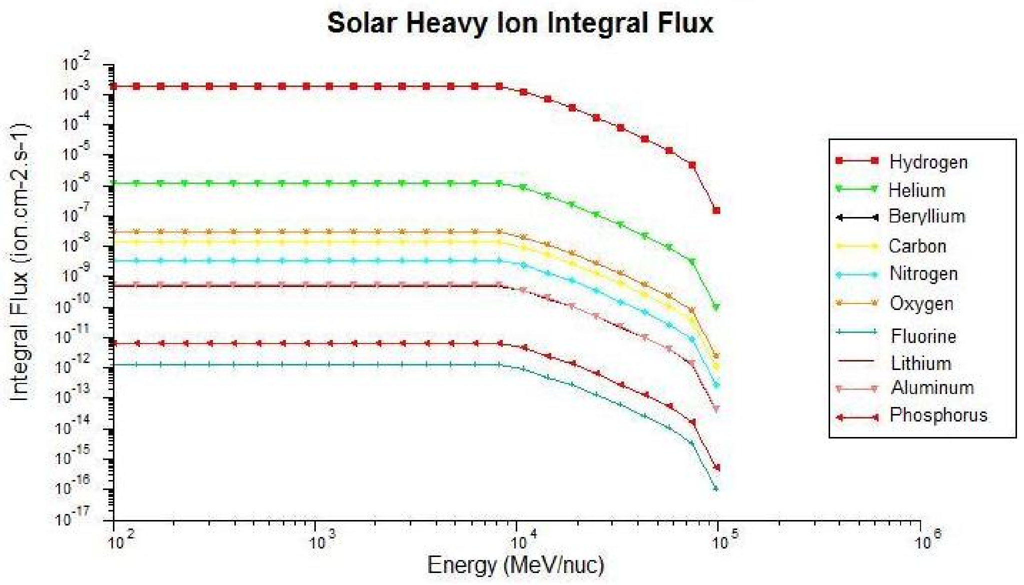

Figure 4.8: Integral fluence versus energy spectra for ions for a five year mission whose one year is in solar minimum and four years are in solar maximum at the 80 % confidence level.

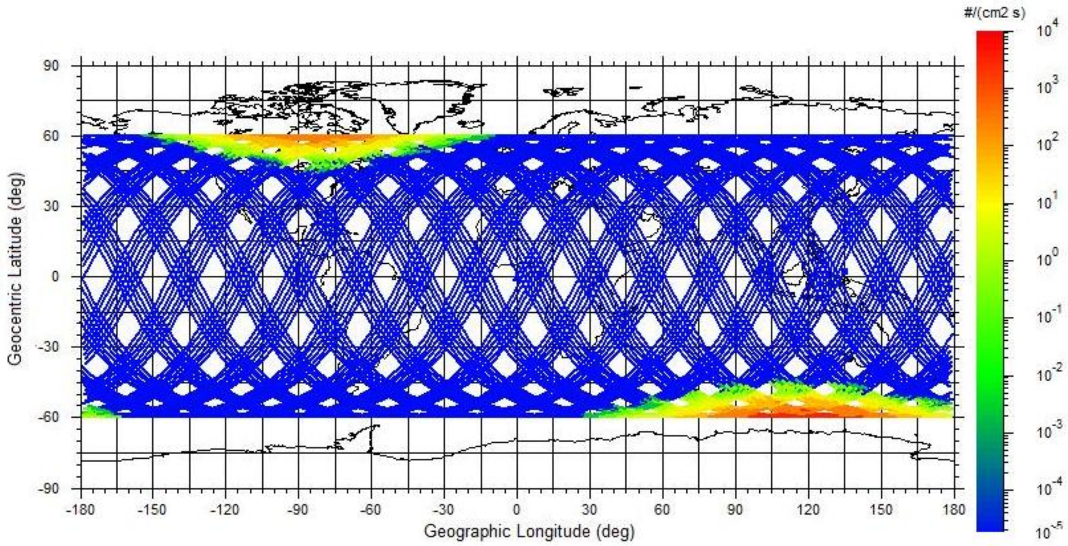

Figure 4.9: World map of integral flux for galactic cosmic rays.

tivity. Galactic cosmic rays with energies smaller than 1 GeV/nuc show a decrease in the flux because of the solar wind. The flux of some elements which contribute the most to the Galactic cosmic rays for both solar minimum and solar maximum in Figure 4.10.

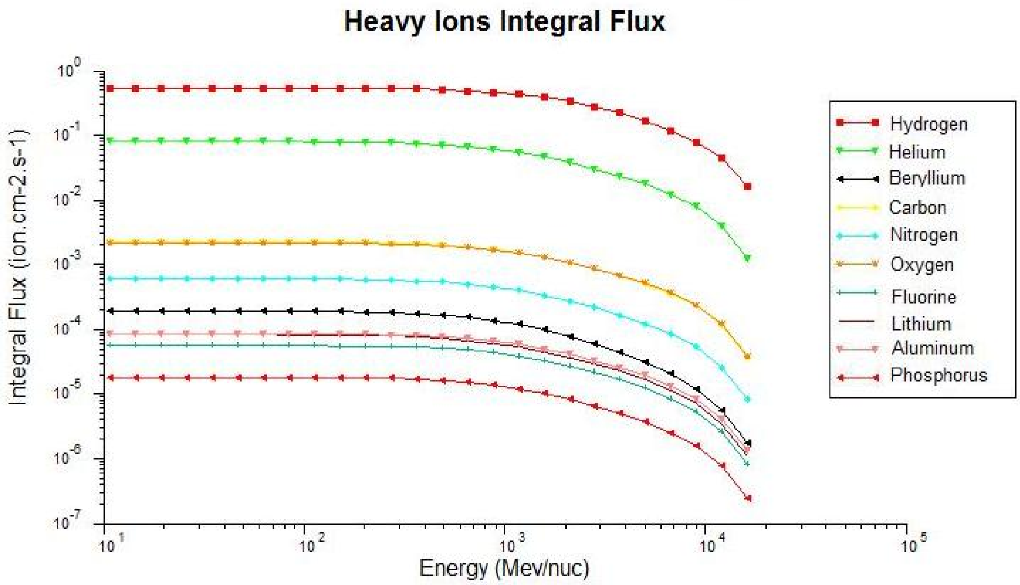

Figure 4.10: Integral fluence versus energy spectra for galactic cosmic rays for a five year mission whose one year is in solar minimum and four years are in solar maximum in 500 km – 700 km altitude.

Dose depth curve presents the top-level ionizing dose environment. Dose was provided as a function of shield thickness in a solid sphere. Trapped and solar particles for different orbital trajectories referred to the total ionizing doses are investigated for a five year mission length starting in 2010 (one year solar minimum and four year solar maximum) presented in Figure 4.11 for a 500 km altitude 60^0 inclination. In addition, for some different inclinations and altitudes of the representative orbits, total doses for a one year mission are summarized in Table A.3 and figured out in Figure 4.12.

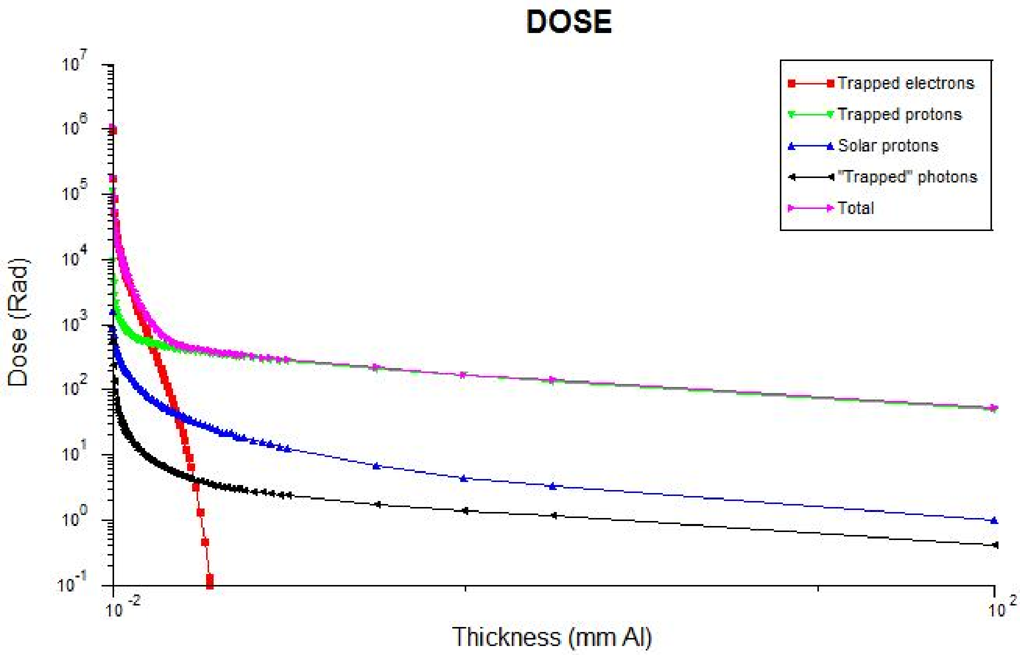

Figure 4.11: Total ionizing dose depth curves for 500 km –700 km altitude with respect to different shielding thicknesses.

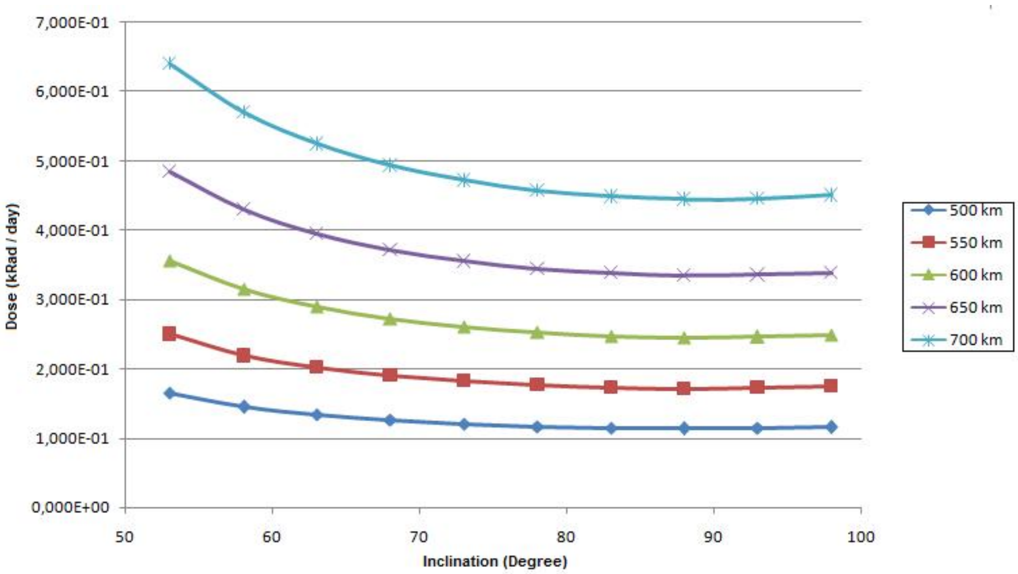

Figure 4.12: Dose changes at different inclinations between 500 km –700 km altitude.

CHAPTER 5

MONTE CARLO SIMULATION FOR TOTAL IONIZING DOSE IN GAMMA IRRADIATION PLANT

5.1 Introduction

Irradiation by Cobalt-60 (Co^{60}) source is not only used in research, industry and agriculture, but also used in total ionizing test. Gamma irradiation plants are built for radiation processing for materials and some devices. For an optimum design and use of these facilities, dose rate distributions depending on the source activity and geometry of the source rack in different locations inside the plant should be known. These distributions are obtained by dosimetric experiments. However, these experiments need huge dosimeters, manpower and they are time consuming. Difficulties are removed by computer calculations with Monte Carlo methods. One of the most exact Monte Carlo methods of computer calculation is Geant4.

5.2 Geant4 Simulation Toolkit

Geant4 is a toolkit that models and simulates the particles through the matter. Geant developed by CERN is an acronym for "**Ge**ometry **An**d **T**racking". It can be used in different applications such as high energy, nuclear, accelerator physics, medical and space science. Geant4 is a program which is the best to use for the particle interaction with matter including visual analysis geometry is a C++ open source software. While calculating the depth of the particle interaction, the possibility to study the motion of particles in a material is provided by Monte Carlo simulation.

Geant4 simulation toolkit constructs the structure geometry by using GDML (Geometry Description Markup Language). Physical properties in Geant4 is provided by XML (Extensible Markup Language). Geant4 includes the geometry, materials, fundamentals particles, generation of primary events, tracking of particles through materials and electromagnetic fields, physical processes, generation of events, storage of events' data, visualization and analyzing the data. It also includes classes. These classes which are shown in Figure 5.1 defines directories and libraries related to Geant4 [73].

Geant4 includes electromagnetic physics that manages lepton, gamma, x-ray, optical and muon physics, hadron physics and variety of theories driven by physics (Compton Scattering, Bremsstrahlung, pair production etc.). Additionally, *Run, Event* and *Track* classes allow event kinematics. The physics of interaction occurring at a given time and a location is determined by *Tracking* class evolving the track's status. In order to reproduce the read-out structure of the detector geometry *Hits* and *Digi* domains are provided. In order to get multiple standards and specialized graphics systems, *Visualization* and *User Interface* are used.

5.3 Gamma Irradiation Facility

The Turkish Atomic Energy Sarayköy Gamma Irradiation Facility [74] is mainly designed for sterilization of medical devices and preservation of food stuff. However, it is also used for determining the total ionizing dose testing for sensitive electronics of some devices. In Turkish Atomic Energy Sarayköy Gamma Irradiation Facility [74] Co^{60} sources are stored under water which is called pool when not in use for irradiation. In the period of no irradiation, sources are stored in a pool whose depth is 6 meters. Sources are elevated up above the pool during the irradiation. Operation parameters and safety systems are controlled by computers. Co^{60} sources take place within an Aluminum storage rack whose thickness is 2 mm. The product for sterilization or preservation to be irradiated is transported by carriers (height = 90 cm,

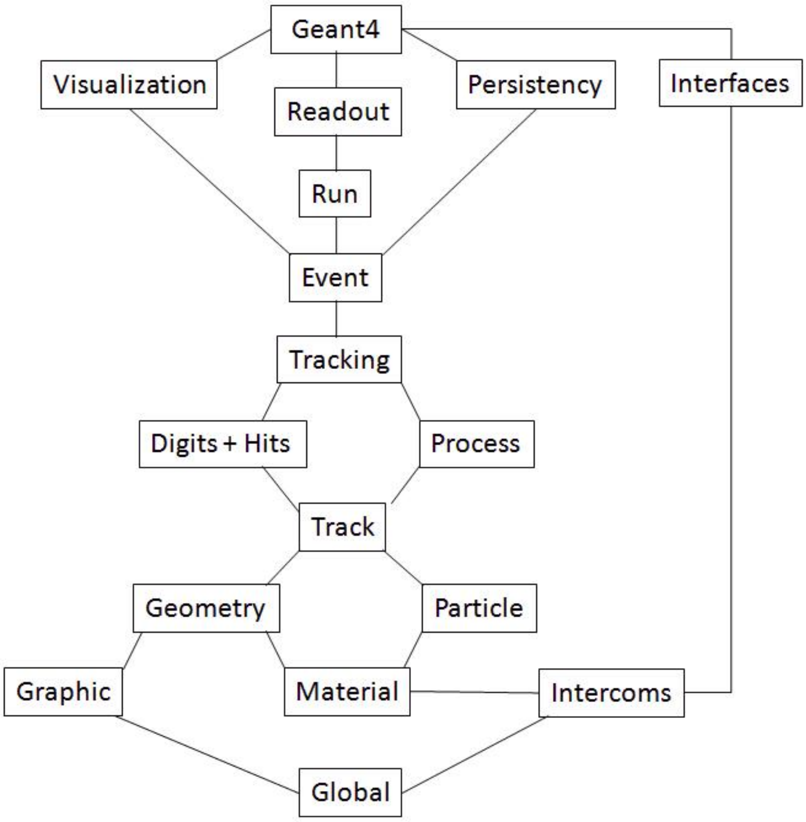

Figure 5.1: Geant4 class diagram and their relationships.

width = length = 45 cm) whose name is tote boxes suspended from conveyor. The thickness of the tote boxes made of aluminum are 3 mm. Irradiation room is shielded by high-density concrete walls whose thickness is 185 cm on the sides and 175 cm on the ceiling. The nominal activity (reported on March 2009) was 6149,4 TBq (166.2 kCi). Figure 5.2 presents a schematic view of the irradiation plant.

5.3.1 Simulation Procedure of the Gamma Irradiation Plant

5.3.1.1 Geometry Definition

The geometry of the irradiation plant was constructed in Detector Construction class. The set-up consists of irradiation room, source, source box, tote boxes, and tally volumes. The irradiation plant of the Sarayköy Gamma Irradiation Plant is a rectangular

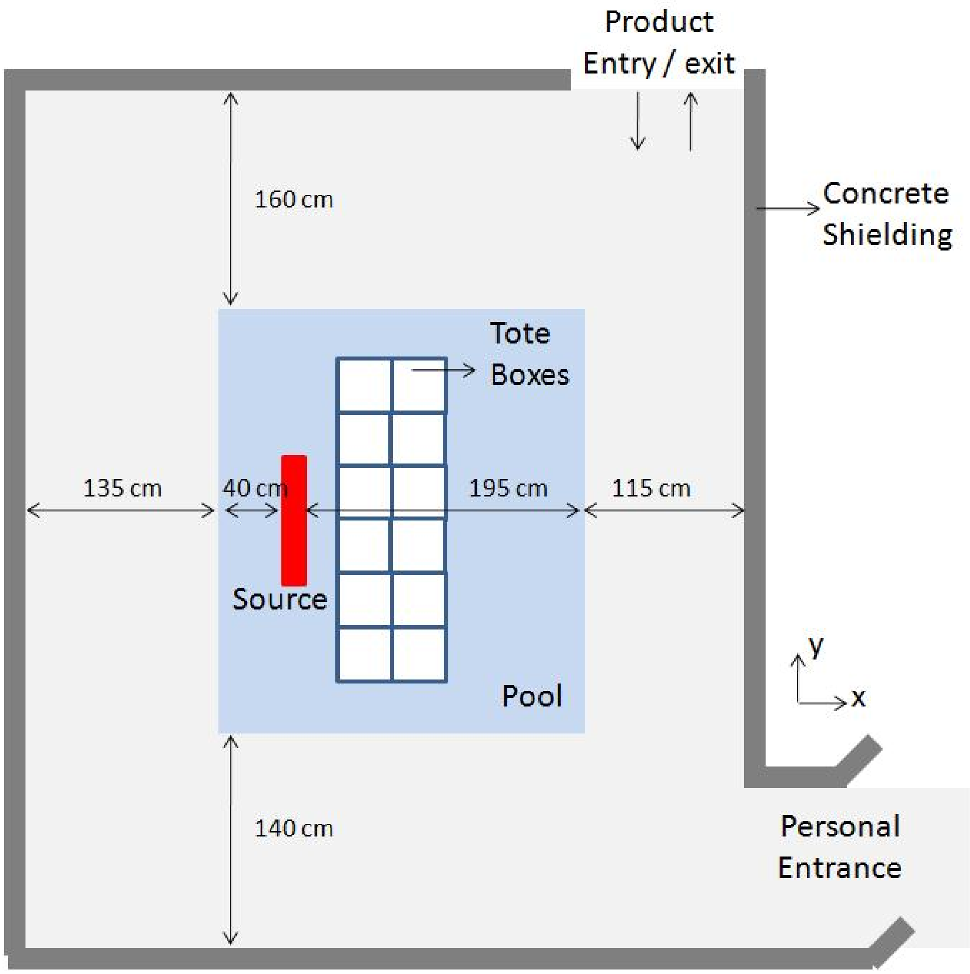

Figure 5.2: Schematic view of gamma irradiation plant.

room whose dimensions are 500x590x400 cm and is called as ”Room” in the simulation. Its dimensions are given as *roomSizeX, roomSizeY, roomSizeZ* for the Cartesian coordinates, respectively. Room was defined inside a ”World” volume which is five times bigger than the room’s dimensions as *worldSizeX, worldSizeY, worldSizeZ*. Room material was defined as air; however, world material was defined as vacuum. The source box ($Source_x, Source_y, Source_z$) is placed inside a 2 mm Aluminum box ($AlBox_x, AlBox_y, AlBox_z$) at their considered positions. In front of the Aluminum box, there are another 3 mm Aluminum tote box carriers whose whole dimensions are 90x270x180 cm. Tote boxes were loaded with air. For dosimeters tally volumes were simulated as spheres filled with water. Since it gives low statistical error for a sufficient total number generated events, and do not affect the non stochastic property of dose definition, the radius of spheres were defined as 4 cm. Dose was obtained by collecting deposited energy in the water spheres along the run. Actual simulation geometry of the gamma irradiation plant is given in Figure 5.3.

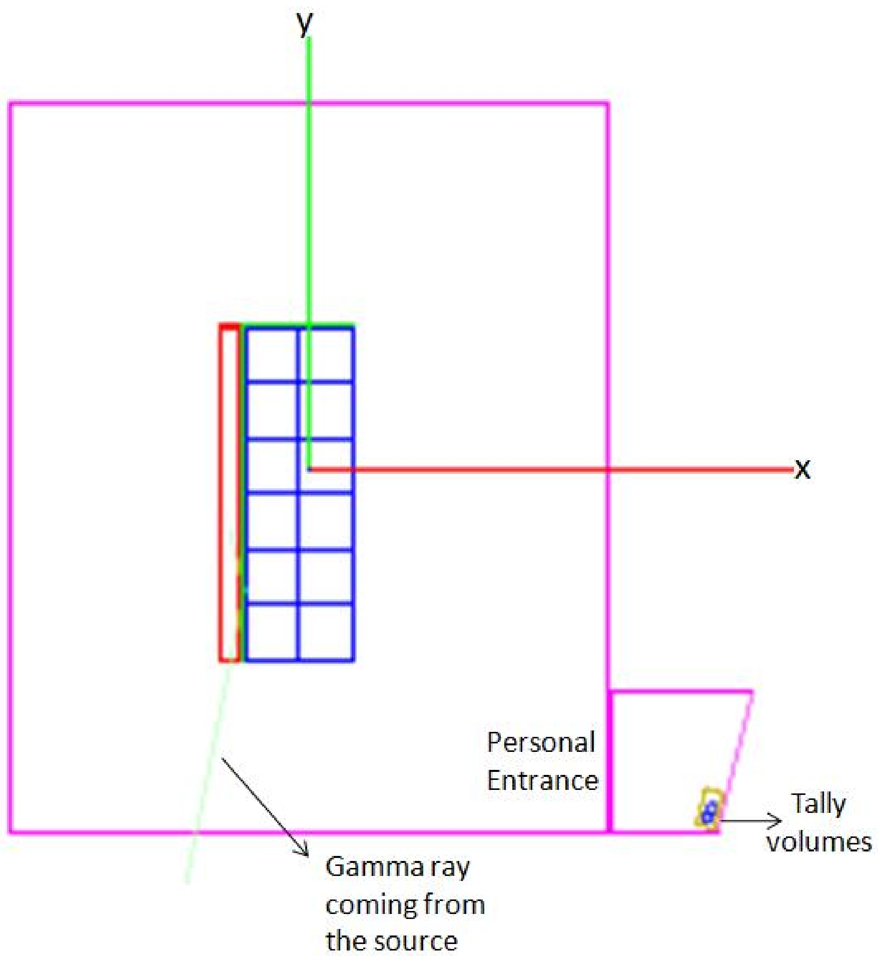

Figure 5.3: Actual simulation geometry of the gamma irradiation plant obtained in Geant4.

5.3.1.2 Physics List and Primary Generator

The particle types and physics processes defined in Geant4 is set in Physic List class. All the standard electromagnetic process which includes photo-electric effect, Compton scattering, pair production, Bremsstrahlung, ionization, multiple scattering and annihilation were introduced. Additionally, radioactive decay process was taken into account. Hadronic process was also defined in Physics List Class, however Hadronic processes were not invoked as default.

Photons were randomly generated from the concerned source in Primary Generator Action class. The event generator is based on the G4GeneralParticleSource (GPS) which allows the user to control all aspects of the initial states of the events. In this simulation, however, GPS were employed to generate the incident beam or the initial radio-isotopes (Co^{60}). By default the incident particle was traveling along the + x-axis and the incident position is 115 cm up from the floor. For the generation of primaries two decay energies of Co^{60} (1.17 MeV and 1.33 MeV) were used. Tally positions, particle energies, their positions, and types and number of events were defined in *"tgipsource.mac"* macro file (See Appendix B). After the definition of the particles, energy deposition was collected in the dosimeters and absorbed dose measurements have been done. Dose was calculated as

$$Dose(Gy) = E_{dep}/m_{tally} \tag{5.1}$$

where E_{dep} is the deposited energy inside the tally volumes which substitutes the simulated dosimeter medium, m_{tally} is the tally mass.

5.3.1.3 Dose Rate Calculation

The current activity reported on March 2009 is 166.2 kCi. Dose rate dD/dt is calculated by transforming photons and electrons deposited energy E_{dep} inside the simulated dosimeter medium of mass m_{tally} during the run of events as follows:

$$\frac{dD}{dt}[\frac{Gy}{time}] = k\frac{E_{dep}[MeV].2A[Bq]}{N_b.m_{tally}[g]} \tag{5.2}$$

where A is the source activity, N_b is the number of particles generated, and k is equal to $1.602x10^{-10}$ is the conversion factor. The factor 2 multiplying A is to take into account of the two photon emission energies of Co^{60}.

5.3.1.4 Main Program

The content of the main program varies according to the needs of a given simulation application. In the main program, the mandatory and optional classes are defined. First, *G4RunManager* object is set. Second, ”Initialize()” instruction of G4RunManager is created. Then, some user action classes commands are defined. The main program for the simulation is placed in Appendix B.

5.3.1.5 Visualization

Detector components, particle trajectories and hits of particles in detector components can be visualized in visualization. The Visualization manager is defined in the main program. In addition, the initialization of the drawing is done via the macro file. For this purpose, it was created *tgipsource.mac* macro file (See Appendix B) for the simulation. While running in interactive mode, the initialization of the drawing is read automatically from the main program. The tracks of the gamma rays are drown at the end of run.

5.3.1.6 End of the Run

The *Deposited Energy*, *Absorbed Dose* and *Dose Rate* values in the test-volumes (tallies) defined in Detector Construction are printed at the end of Run, in the units of MeV, Gray and Gray/time. In the simulation, dose rate calculations were done for 3 weeks for different four dosimeters which were placed in the personal entrance of the room in different positions shown in the Figure 5.4.

Since the tallies were in the personal entrance, incoming rays from the source have been transmitted with a certain solid angle. In this manner, incoming rays were di-

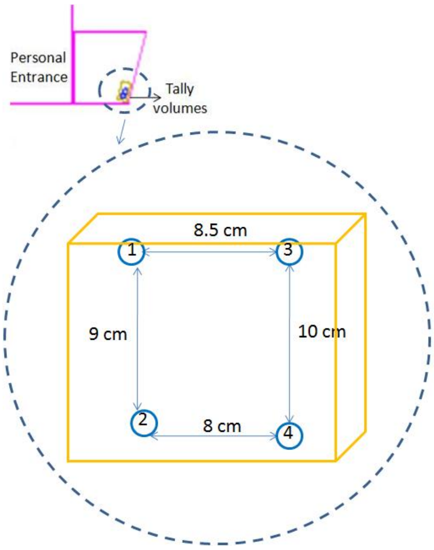

Figure 5.4: The front view of dosimetry positions for the tally volumes created in Geant4

rectly transmitted to the tally volumes. The results obtained from the certain solid angle were multiplied with a factor in order to get real results so that the incoming rays were determined as isotropic point source. In the following, experimental dose rates and calculated dose rates were compared. Experimental dose rates were obtained from the Total Ionizing Test results in November 2008.

Table 5.1: Comparison between measured and predicted dose rates at four points.

Tally Number	**Experimental Dose Rates** (kGy/3 weeks)	**Simulation Dose Rates** (kGy/3 weeks)
1	0.61	0.72
2	0.81	0.97
3	0.56	0.47
4	0.81	0.85

5.3.1.7 Results

Geant4 has been used for the simulation of gamma rays in Sarayköy Gamma Irradiation Plant. Taking into account the statistical uncertainty of dosimeters ($\leq 12\%$) and simulation ($\leq 8\%$), it can be concluded that the experimental and simulation results are in good agreement. The simulation model provides an accurate dose mapping inside the radiation plant. Dose rate variations predicted before total ionizing dose testing can be estimated. After predicting the amount of dose required during the total ionizing test, the suitable place where the test occurs can be estimated from the simulation results.

CHAPTER 6

TOTAL IONIZED DOSE AND SINGLE EVENT EFFECTS TESTING

6.1 Introduction

The sensitivity of electronic devices to radiation is often very changeable and it is not possible to use solely the theory to predict the effect on a device of a given exposure to radiation. Actual irradiation tests can be evaluated as an integral part of a system. However, Tests can sometimes be performed on each batch of parts. In this chapter, it is aimed to provide test standards, total ionizing testing, single event effect testing, and their test sources.

6.2 Test Standards

National and international standards have been developed by Institutes in the USA and Europe for the assessment of devices under radiation. These standards can be classified : ESA/SCC and ECSS Specifications (Europe), BS 9000 specifications and CECC (Europe), MIL-STD specifications (USA), ASTM specifications (USA) and Electronic Industries Association EIA (USA). These standards define the requirements applicable to the testing of sensitive electronic devices. The most commonly used test standards are ESA/SCC and ECSS Specifications and MIL-STD specifications. Despite the MIL-STD specifications were written for military applications, they have also been adapted for space applications. ESA/SCC and ECSS Specifications are only applicable for space applications. Both specifications define the test conditions and qualifications of the systems which are used in space missions in different ways.

Test standards of radiation test procedures which were used for testing in this thesis are *ESA/SCC Basic Specifications No:22900: Total Dose Steady-State Irradiation Test Method* and *ESA/SCC Basic Specifications No:25100: Single Event Effects Test Method and Guidelines* developed by the ESA Space Components Coordination Group. The purposes of these test standards are to define the effects of total dose ionization and displacement relevant to the space environment and the usage of proton and heavy ion accelerators for single event effect testing, respectively.[75]

6.3 Device Under Test (DUT) Parameters

- Technology: 8-bit micro-controller
- Program Memory Type : 64KB Flash Memory
- RAM Memory : 3.328 bytes
- CPU Speed: 10 MIPS (million instructions per second)
- Channels: 16 Channels Analog-to-Digital Converter, Resolution 10 bit
- External Memory Access: Up to 2Mb of capacity
- Frequency: 40MHz Max Speed
- Temperature Range : -40 C^0 to 125 C^0
- Operating Voltage: 2 V to 5.5 V
- Package: TQFP (thin quad flat pack) 80 pins

6.4 Total Dose Testing

6.4.1 Total Ionizing Dose Test Sources

For investigating the basic mechanism of radiation effects or for simulating the total dose response of electronics in the natural space environment, the most common laboratory sources are Co^{60} sources and X-ray sources. Gamma rays whose energies are 1.17 MeV and 1.33 MeV are emitted from Co^{60} sources. Although, the space radiation environment consists of electrons and protons, the ionizing radiation environment is tested with energetic gamma rays. Since Co^{60} sources emit gamma rays with an average energy 1.25 MeV at dose rates up to 400 rad/s (4 Gy/s), the conservative estimation of the space radiation environment are given by gamma rays, [76]. In order to simulate low dose rate total dose effects, apart from Co^{60} source, Cesium-137 (Cs^{137}) source can be used. Cs^{137} sources emit gamma rays with an average energy 0.66 MeV at dose rates up to 0.01 rad/s (0.0001 Gy/s). Apart from Co^{60} sources, another common type of laboratory source is X-ray. Laboratory X-ray sources can achieve dose rates from 100 Rad/s (1 Gy/s) to 2000 rad/s (20 Gy/s) with the energy of 10 keV.

In addition to low dose rate sources, high dose rate sources such as electron accelerators (LINACs) and proton cyclotrons are also available. Electron LINACs are pulse type of radiation sources with energies from 10 MeV to more than 40 MeV and dose rates greater than 10 Grad/s (0.01 GGy/s) can be achieved. Proton cyclotrons can have energies from 40 MeV to 200 MeV. Dose rates 1 Mrad/s (10 kGy/s) can be obtained from proton cyclotrons.

6.4.2 Testing and Results of Total Ionizing Test

The total dose test was performed in Turkish Atomic Energy Agency at Sarayköy, Ankara according to ESA specifications [77]. The DUT whose properties were described above was tested by using gamma ray Co^{60} source at the dose rate 3.8 krad/h

(38 Gy/h). The total dose test was performed for the DUT according to the irradiation test plan. The sequence of the test plan for total ionizing dose can be given in Figure 6.1 [77]:

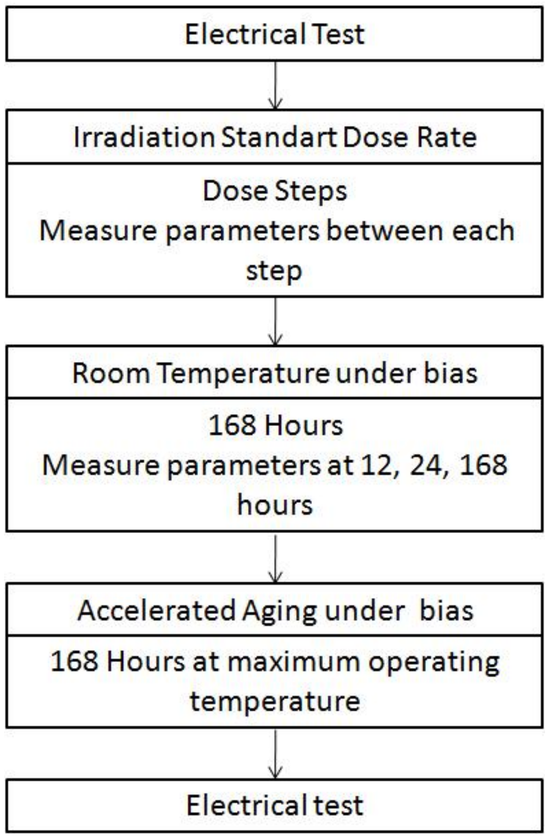

Figure 6.1: Flow Chart of the test method

Standard ESA procedure which was followed during the test can be given as in the following:

1. Initial electrical characterization of the components at room temperature which was 24 °C has been monitored during the irradiation.

2. Radiation source and bias of components set. During the test the components were under bias.

3. Components were irradiated until failure. Three exposures were made with monitoring of electrical parameters. The dose rate should be between 3.6 to 36 krad/h. It was used 3.8 krad/h dose rate in the test. Three irradiation steps of 1 kRad (10 Gy), 3 kRad (30 Gy), 30 kRad (300 Gy) were made.

4. Post irradiation electrical characterization of exposure were made. Component parameters were also measured.

5. After completion of final exposure, components were also retested and underwent annealing for 12, 24 and 168 hours (1 week) at 25 °C.

6. After annealing, ageing is performed. Components were baked at maximum operating temperature under bias for 168 hours.

7. Final electrical characterization of the components at room temperature which was 24 °C has been monitored.

When the components were in place for in-situ radiation test, they were checked for proper interconnections, leakage and noise level. The components were monitored for oscillations and current drain. The components remained in place on the test circuit board. In addition, the test circuit board remained in its irradiation location throughout the irradiation and measurement sequence. In order to determine the proper operation and stability of the measurement, a control device was measured with the measurement system before the insertion of the components and again upon completion of the irradiation and measurement. Electrical parameters were tested in three conditions: a. I_{cc} clocked not running, b. I_{cc} not clocked, and c. I_{cc} clocked and running. Current consumptions (I_{cc}) for the conditions were plotted in Figures 6.2, 6.3, and 6.4, respectively[1].

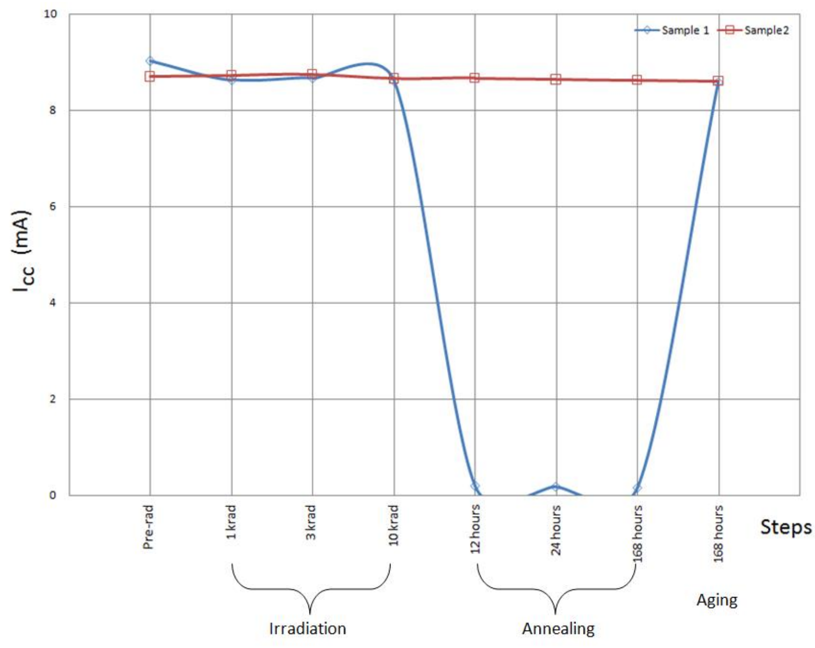

Figure 6.2: Current consumption in condition a.

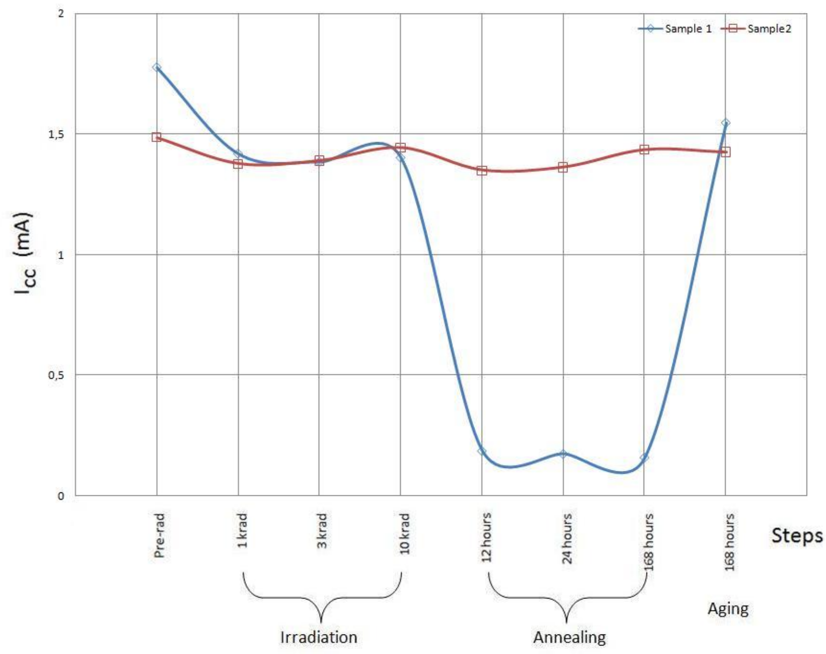

Figure 6.3: Current consumption in condition b.

[1] Total Ionizing Test Report data were used.

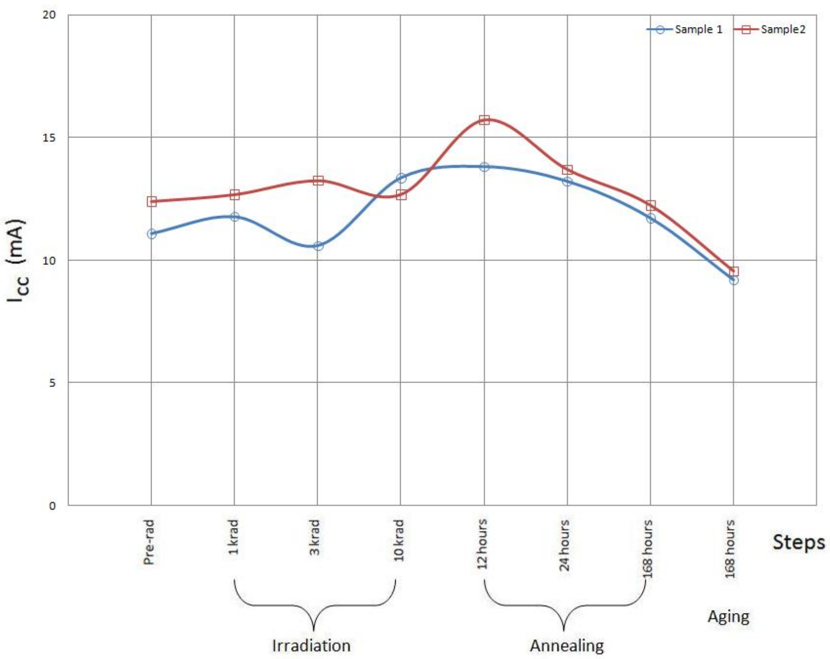

Figure 6.4: Current consumption in condition c.

As seen in Figures, after 10 krad (100 Gy) both components which were tested according to the irradiation test plan lost their programming and they were reprogrammed. During annealing, Sample 1 lost its program and was not able to reprogrammed after aging. However, Sample 2 lost its program after 12 hours of annealing but was reprogrammed. Both components were working after aging. It was understood that the components can be used up to 3 krad.

6.5 Single Event Effect Testing

6.5.1 Single Event Effects Test Sources

In order to characterize heavy ion and proton induced single event effects, particle accelerators are widely used at accelerating potentials up to 300 MeV. In particle accelerators ion species, energies and flux vary. In heavy ion testing energy and particle specie must be well-defined. Heavy ion accelerators enable us to use uniform beam flux which varies between $10^2 - -10^5 ions/cm^2.s$ over the test sample. In order to evaluate single event effects, it is required an energetic heavy ion source with LET values ranging from about 10 to $45 MeVmg^{-1}cm^2$. For investigating the behavior of a device around threshold LET, low LET values are required. However, in order to determine the limiting cross section or saturated error rate, higher LET values are used. The device to be tested is placed on a target which contains silicon detectors in front of the ion beam. Generally, the target where the device to be tested is placed provides to tilt with respect to the beam in order to allow the path-length of the ion beam through the device to be varied.

In order to achieve a single event effects testing, another method is the use of fission products from a small radioactive Californium-252 (Cf^{232}) source. The average LET value of the fission products is 434 $MeVmg^{-1}cm^2$. This value is sufficiently high to get the limiting cross section. However, the LET value can be reduced to 15-20 $MeVmg^{-1}cm^2$ by using foils or gases. On the other hand, this range is not low enough to determine the threshold value for some devices. The main advantage of using the Cf^{232} source is its low cost, simplicity, and flexibility.

In addition to the previous sources, laser light is also used for single event effect testing. Single event effects can be tested using short, high-intensity pulsed of laser light.

6.5.2 Testing and Results

Single Event Effect Testing was performed in a heavy ion accelerator facility of LNS (Laboratori Nazionali del Sud) [78] according to ESA specifications [79]. The device was exposed to beams Ar^{40}, Kr^{48}, and Xe^{129} with the range of 400 MeV/nucleus, 1680 MeV/nucleus, and 2580 MeV/nucleus with increasing LET values, respectively at different incident angles ($0^0 - 40^0$). The experimental setup (Figure 6.5) located in air and it consisted of *thin scintillator* which is a device for detecting and counting scintillations produced by ionizing radiation for online flux monitoring, *two stages* where DUT and CsI scintillator were mounted, *data acquisition* (DAQ) *system*, *two controlling DAQ* and *stage movements*.

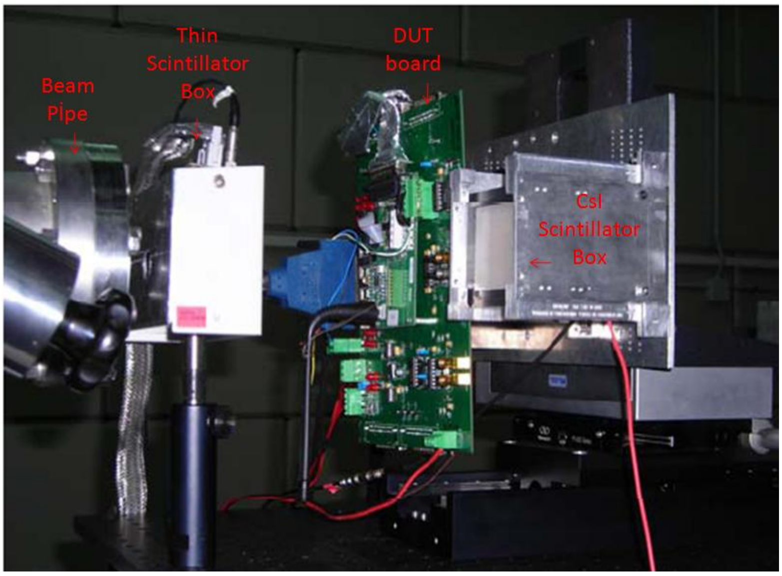

Figure 6.5: Single Event Effects test setup.

The beam profile was measured for each ion type prior to start the irradiation with a given ion type. For this purpose, a photosensitive foil as showed in Figure 6.6 was used to center the beam with respect to the thin scintillator and DUT which is behind the thin scintillator. X and Y axis beam profiles were then obtained by scanning the impressed foil and elaborating the scan data with ad-hoc software.

The ion flux (fluence) monitoring was performed online through a 30 μm thin scintillator. The calibration of the thin scintillator was done for each ion type by counting the both the thin scintillator and a CsI scintillator with the last placed at exact position of DUT to be tested. Once the calibration was completed, the DUT was moved under the beam axis and the data taking was initiated.

In order to obtain LET values for different ion types and energies, Geant4 was used [73]. Experimental setup was realized in Geant4 which is represented in Figure 6.7.

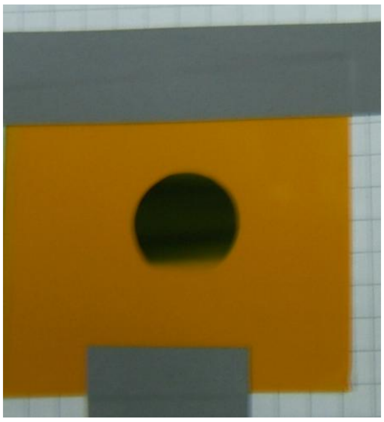

Figure 6.6: Beam profile on the photosensitive foil.

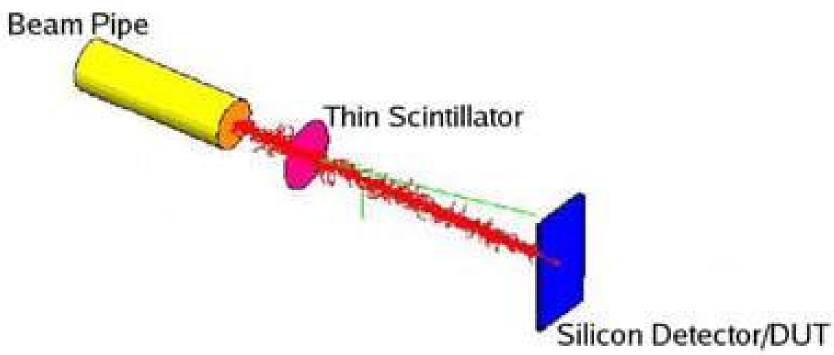

Figure 6.7: Single event effects test setup simulated by Geant4. The direction of the beam is from left to the right.

LET calculation was done by using the energy released and its relative range in bulk silicon. The LET cross section can be given as in the following:

$$LET = \frac{1}{\rho}.\frac{dE}{dX} \tag{6.1}$$

$$\sigma = \frac{N_{SEE}}{Fluence.Cos(\theta)} \tag{6.2}$$

where ρ is the density of silicon and $\frac{dE}{dX}$ is the energy released per unit length. LET is given in the units of $[\frac{MeV.cm^2}{mg}]$. σ is the cross section is given as $[cm^2]$, N_{SEE} is the number of upsets. The single event upset behavior of the DUT was monitored by comparing a memory pattern with a duty cycle of 1 MHz while irradiating the DUT. When the LETs were not directly available, the device was tilted to give an increased effective LET. The Table 6.1 summarizes the data parameters of the DUT to trace cross section versus LET curve [2].

Table 6.1: The data summary of the device under test for single event effects testing.

Ion Type	Incident Angle (Degree)	LET ($MeV.cm^2/mg$)	Flux ($\sharp/cm^2.sec$)	Effective Fluence ($\sharp/cm^2$)	Cross Section (cm^2/bit)	Total Effective Fluence ($\sharp/cm^2$)
Ar^{40}	0	8.351	4.83E+03	1.77E+07	1.13E-07	1.77E+07
Ar^{40}	0	10.97	4.18E+03	1.17E+07	2.18E-05	1.17E+07
Kr^{48}	0	31.29	2.18E+02	2.00E+05	6.11E-04	2.00E+05
Xe^{129}	0	63.62	1.99E+01	1.33E+04	1.12E-03	1.33E+04
Xe^{129}	40	83.05	2.01E+01	1.33E+04	1.20E-03	1.74E+04

The experimental cross section curve is either defined by a table of cross section versus effective LET values shown in Table 6.1 or fitted to a four parameter Weibull function as shown in Figure 6.8.

The four parameter Weibull function is given by [80]

$$\sigma = \begin{cases} \sigma_s.[1 - Exp(-(\frac{E-E_0}{W})^S)] & (E > E_0) \\ 0 & (E \leq E_0) \end{cases} \quad (6.3)$$

where E_0 is the threshold energy in MeV, σ_s is the saturation cross section in cm^2/bit, W is the width of the rising portion of the curve in MeV and S is the power that determines the shape of the curve.

Based on the test and analysis, the saturation cross section and threshold LET value derived from the parameters of Weibull fit to cross section versus LET data were obtained for the device. Saturation cross section is $2.2210^{-9} cm^2/bit$ and the threshold

[2] Single Event Effects Test Report data were used.

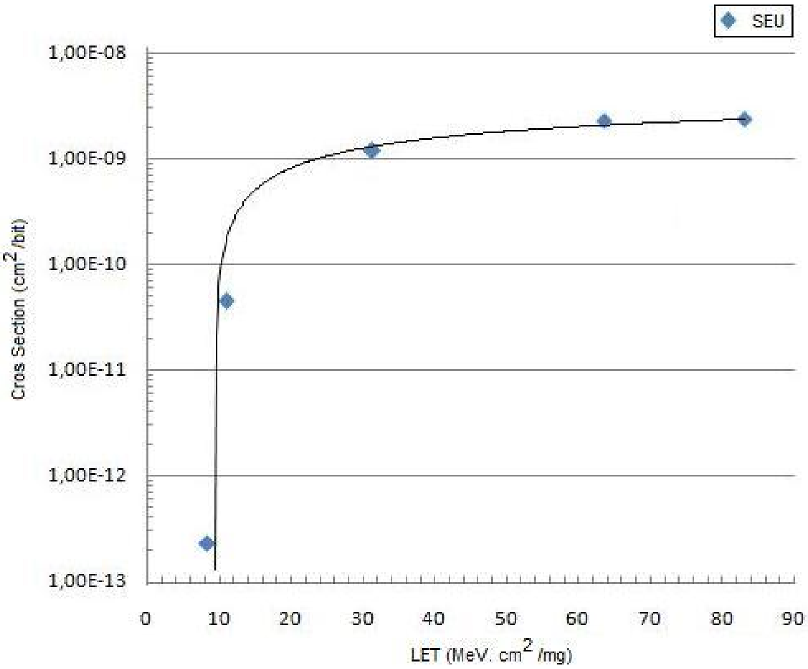

Figure 6.8: Single event upset cross section per bit versus LET curve.

LET value is equal to $9.8 MeV.cm^2/mg$. According to Table 3.1 in Chapter 3, results showed that the device which was exposed to the test is vulnerable to single event effects.

CHAPTER 7

THE RADIATION HARDNESS ASSURANCE FOR IRRADIATION OF ELECTRONIC COMPONENTS IN AIR

7.1 Introduction

The LNS Superconducting Cyclotron (CS), is a compact, strong focusing three-sector machine. The pole radius is 90 cm and the magnetic field at the center ranges from 2.2 to 4.8 T. This is obtained with superconducting Nb-Ti coils cooled down to 4.2 K cooled with Liquid Helium. The expected maximum energies of the machine are of 20 MeV/nucleus for the heaviest ions and 100 MeV/nucleus for fully stripped light ions. The bending limit is $K_b = 800$ and the focusing limit is $K_f = 200$. The relatively high energy of the beams (for this study 20 MeV/nucleon) allows the irradiation of components in air which is also used as a degrader. The selection of the ion species used in SEE studies is done by taking into account the easiness of beam changing operation and at the same time the necessity to cover uniformly a LET interval as large as possible. Hence four noble gases beams ($Ne^{20}, Ar^{40}, Kr^{84}, Xe^{129}$) all with 20 MeV/nucleus energy were selected for operation. A careful evaluation of energy loss in air and of the energy spread at DUT surface is carried out through a full Monte Carlo simulation of the test setup and comparing the results with data.[1]

[1] This work was submitted in Radiation Effects on Components and Systems as Paper Number 1112.

7.2 Beam Flux Measurement

The measurement of beam flux and uniformity is one of the ingredients for the calculation of SEE cross-section. According to the ESA standard ESCC 25100 [79] these measurements should be done with an accuracy of ±10%.

At LNS, extraction in air of ion beams is performed and the flux dosimetry setup is resided in air; additionally air is used as a degrader in order to adjust LET values. A picture of the dosimetry measurement setup is shown in Figure 7.1.

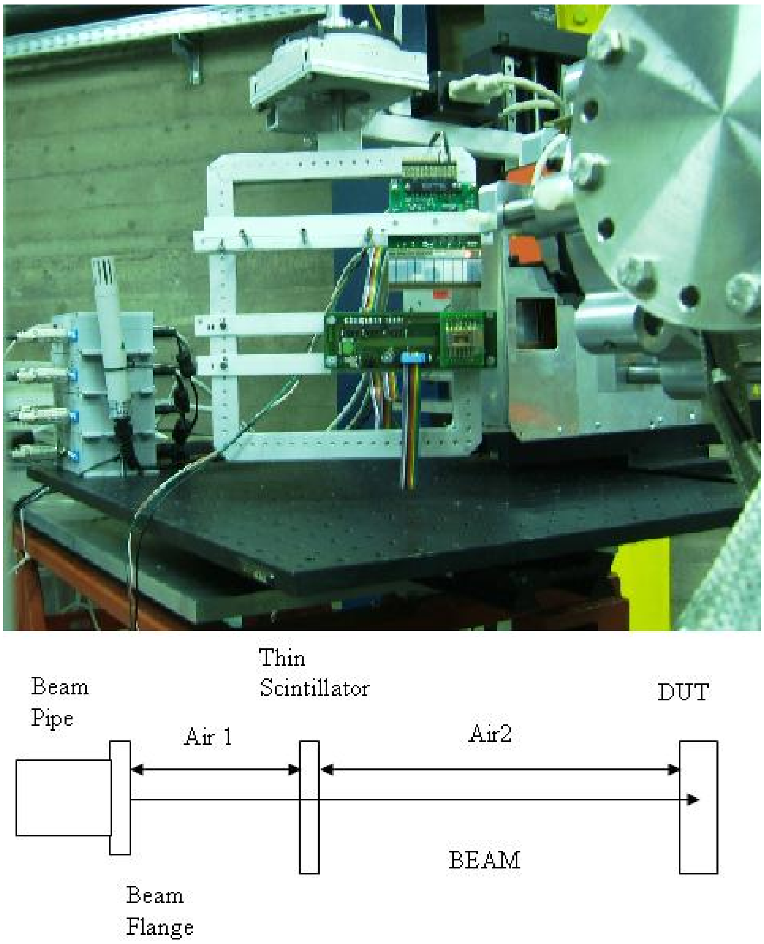

Figure 7.1: Picture and scheme of beam flux measuring setup. Thin scintillator is mounted on two arms attached to the beam flange. The supporting frame holding a DUT is also shown. Air1 has a fixed value (5 cm) while Air2 can change from 5 to 30 cm.

The setup consists of a thin scintillator counter (NE102A of 50, 100 or 2000 μm thickness) read out by a photomultiplier just after (5 cm distance, this distance is referred as Air1) the beam exit into air. The scintillator is inserted into a metallic box with variable size beam hole to allow the adjustment of the beam size. The DUT is placed onto a supporting frame (DUT holder) at a variable distance from the scintillator (this distance may vary from 5 to 30 cm and is referred as Air2). The DUT holder is capable to move in XYZ directions and to rotate around a vertical axis. On the same structure close to DUT holder a double sided, 1.5 mm thick microstrip detector (500 μm readout pitch and 3x3 cm^2 active area) is mounted for energy, fluence and beam profile measurements. Because of its thickness the silicon detector absorbs the entire energy of all ions. The stopping range in silicon is, for all ions, at least 30 μm, in accordance to the minimum penetration depth required by the ESA standard ESCC 25100 [79].

The dosimetry and SEE testing setup includes two additional important features. A laser device is used to measure the distances in Z (beam) direction (namely Air2) with 200 μm position accuracy. Such level of accuracy in measurement of the relative distances (i.e. silicon detector surface to DUT surface, DUT surface to beam exit in air etc.) is important to minimize the systematic uncertainty on LET value in silicon, as will be described in Section 7.3. The other feature of the setup is a custom module (SELDP, Single Event Latchup Protector and Detector [81]) built specifically to monitor the current drawn on power line of a DUT. The SELDP cuts the power supply to DUT for an adjustable time duration whenever the current drawn by DUT exceeds a preset current limit. This both protects DUT from burnout because of Single Event Latchup (SEL) effect and registers the number of SEL occurred by incrementing a counter.

The measurement strategy is the following: prior to beam period, an optimization of LET values is performed using Geant 4 [73]. This optimization adapts customer's request of LET values with available ion species, Air2 values and tilting angles the result of these calculation are presented in a look up table. At the beam site, a calibration run of the beam is made for each energy point present in this list and during irradiation the beam parameters are measured. During calibration run, under the beam the scintillation counter and the silicon detector are placed. The scintillator acts as a counter of ions crossing the detector. Careful adjustment of the counting threshold is performed in order to have maximum efficiency.

During calibration runs both detectors are on beam and the following measurements are performed:

- Energy of the ion by measuring the charge collection of each ion hitting the silicon strip detector. This measurement is important to determine the uncertainties on LET measurement and the percentage of fragmented ions which are present in the beam.

- Beam profile: The flux is measured by using information on the number of counts per strip per unit time and the position of each hit. From this measurement, the flux and the fluence during the calibration run can be determined. Typical beam profiles from online monitoring and from reconstructed data are shown in Figure 7.2 and 7.3.

- Comparative measurement of the counting rate in the scintillation counter and in the silicon detector. This measurement is performed by recording the counting rate in the scintillator counter and in the silicon detector in order to have a correlation between the flux on the silicon sensor and the counting rate of the thin scintillator. The ratio between the two measurements is used to measure flux and fluence when the DUT will be on the beam in place of the Silicon strip detector.

During the actual irradiation run, the scintillator is replaced with the DUT (same Air2

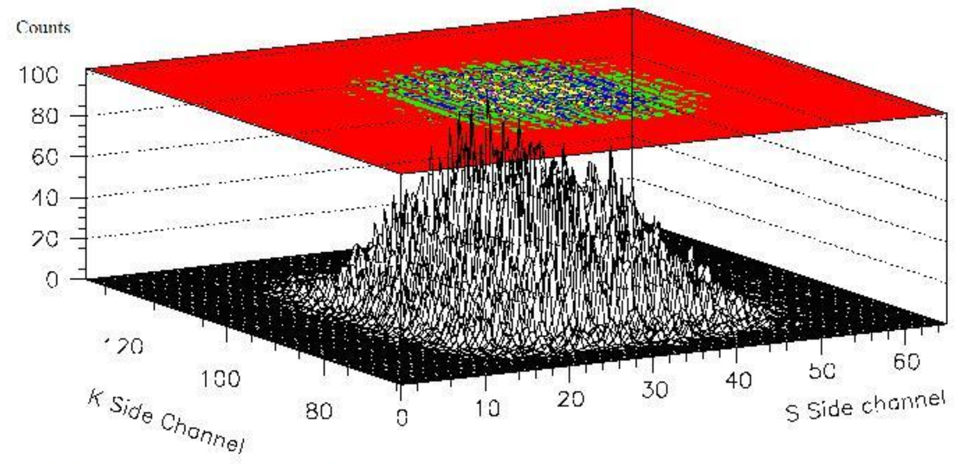

Figure 7.2: The online monitoring of beam parameters. The beam profile is shown in detail. S-side is the horizontal coordinate while K-side is the vertical coordinate. Each channel corresponds to 0.5 mm (strip pitch of double sided silicon detector).

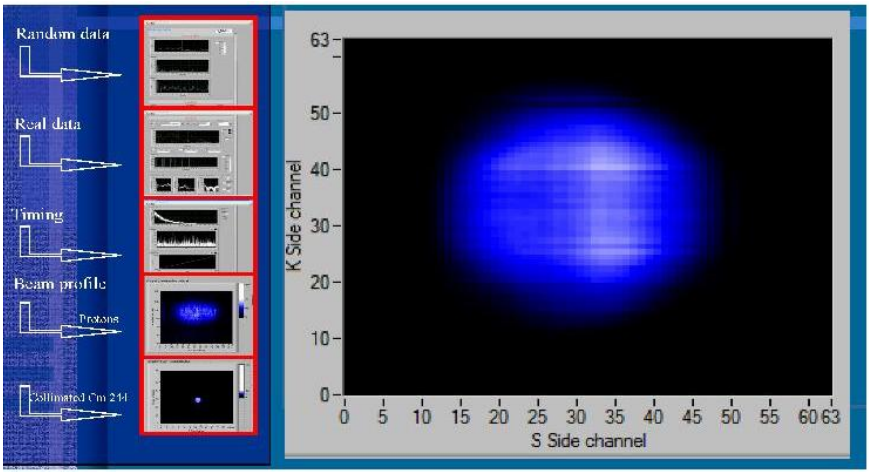

Figure 7.3: The online monitoring of beam parameters. The beam profile reconstructed from data.

distance). The results of beam profile and comparative (scintillator-silicon) measurements in order to calculate the flux, the fluence and the energy measurement are used to have an estimation of the errors on LET.

The energy spread provided by the simulation and the silicon detector data are in good agreement. This spread is below the 10% of the target energy value indicating the good beam purity and full control of the systems parameters (see Table 7.1).

Table 7.1: The ion and corresponding LET values and related errors according to Geant4.

Ion/LET ($MeV.cm^2/mg$)	**Error on LET** ($MeV.cm^2/mg$)
Ne^{20}/3,7	0,1
Ar^{40}/13,13	0,2
Kr^{84}/30,6	0,7
Ne^{129}/52,9	0,8

7.3 Systematic Uncertainty Evaluation for SEE Cross Section Measurements

A careful evaluation of systematic uncertainty is necessary to estimate overall error introduced on LET and on fluence values. Definition of LET and cross section is given as in Equation 2.6 where ρ is silicon density.

Systematic uncertainties on LET values are due to:

- Uncertainties on distance (air thickness) measurements. This is done with a 200 μm accuracy laser system only once during the initial calibration phase. All other positions are relative to that point with submicron precision 4-D stage (X,Y,Z, Theta).

- Fragmentation in air. It is negligible (i.e. $< 10^{-4}$ for 20 MeV/n Ar^{40} after 15 cm of air) according to Geant4 simulation performed using ”binary light ion cascade” and ”Wilson abrasion” models. Fragmentation is also measured during calibration. The amount of fragmentation measured is in agreement with monte-carlo predictions.

- Errors on the determination of energy deposited and range in the DUT by Geant4 simulation; the energy distribution from Monte Carlo has less than 3%

error at FWHM (see Table 7.1), and there is a good correlation with the charge measured by the silicon detector, which provides the possibility to convert the charge values to deposited energy. The correlation between charge collected in silicon and simulated deposited energy for different air thicknesses for Ar^{40} is given in Figure 7.4. In this figure the values are obtained by changing the Air2 thickness (not the beam).

- Positioning of beam spot to the center of DUT and correction of non uniformity of beam over the beam spot. Figure 7.5 shows a typical beam spot and DUT dimensions. This error includes a 180 μm contribution from the silicon detector spatial resolution, as well as a 300 μm one from the accuracy of the DUT mounting on the holder frame; the two contributions are summed in quadrature since they are independent.

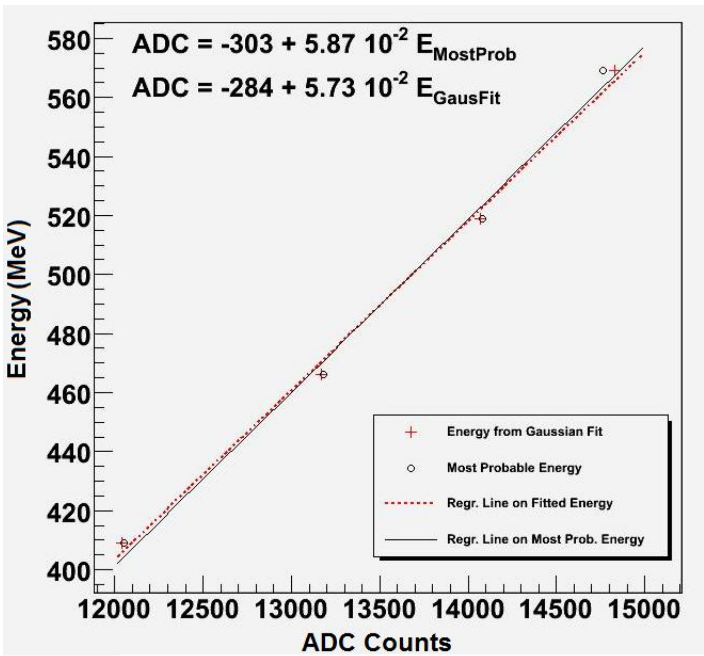

Figure 7.4: Correlation curves between deposited in silicon (ADC counts) and simulated energy release (MeV). The two data sets and curves refer to different ways to estimate energy from Monte Carlo distribution: circles use the most probable value taken from energy histogram, crosses use mean from a gaussian fit.

The detailed analysis of errors have shown that the overall error on determination, both of fluence and of LET, is less than 4% which is well below the upper limit (10%) required by ESCC 22500. The Table 7.1 lists the overall systematic uncertainties on LET values for different ion species at 10 cm of Air2.

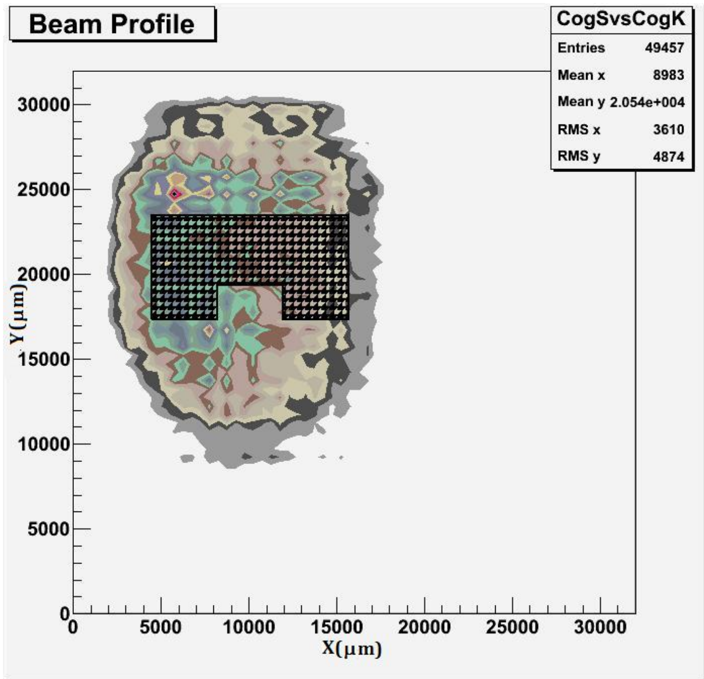

Figure 7.5: Beam spot is centered over DUT surface. From this profile, one can extract the real fluence distribution over the DUT surface. The beam spot positioning accuracy is at most 400 μm.

7.4 Comparison With A Benchmark Setup

In order to measure the consistency of the experimental measurements with other measurements done in other beams, a benchmark setup developed by ESA/ESTEC [82] named SEU monitor was used. This setup measures the number of SEU events on a Atmel AT60142F-DC1 SRAM which is a component that has a well known SEU cross section versus LET curve (measured in several facilities) and is Latchup immune. The software of this test setup, once the data on LET and fluence are inserted, calculates immediately the cross section versus LET and displays the result on a graph where previously measured values are displayed. Figure 7.6 shows our results compared with these values measured in other facilities. As shown the results are in good agreement with the previous measurements.

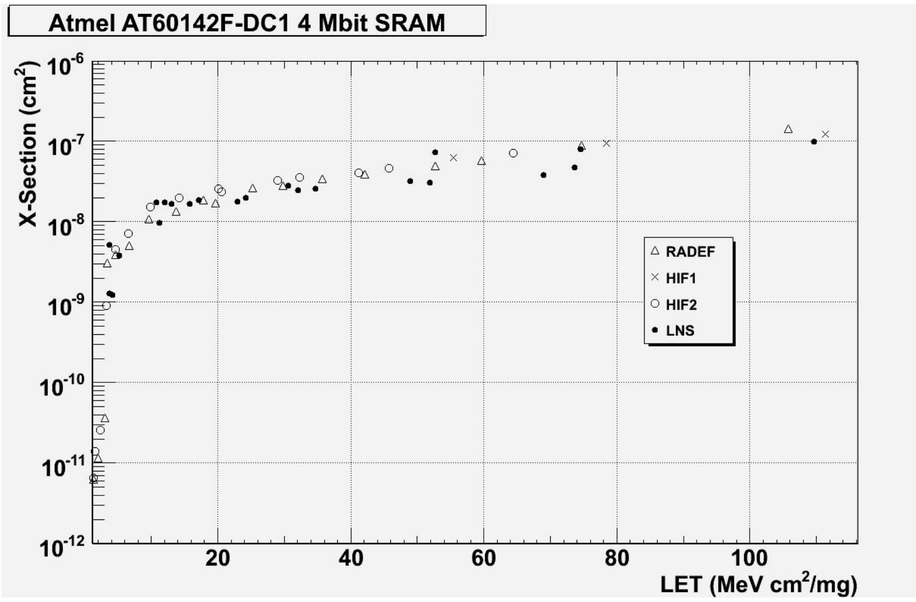

Figure 7.6: Cross section in cm^2 versus LET in $MeV.cm^2/mg$ of Atmel AT60142F-DC1SRAM measured with our setup and with several other beam facilities.

CHAPTER 8

SUMMARY and CONCLUSION

This thesis constitutes the first comprehensive study of ”Radiation Hardness Assurance” on space electronics in Turkey. The principle objective of this research has been to investigate the behavior of space radiation environment, modeling, radiation transport simulation, total ionizing dose and single event effects testing of electronic devices used in a space mission, in order to determine their suitability for the construction for use in space.

The Earth is surrounded by a magnetosphere, shaped by the dynamic interaction between the solar wind and geomagnetic field. The structure of the Earth’s radiation environment is dominated by the magnetic field. The Earth’s magnetic field acts as a partial shield against charged particles which come from inside and outside the Solar System. There are three main environments of concern for space electronics: trapped radiation, galactic cosmic rays and solar flare particles.

Van Allen trapped radiation belts are a very serious threat to space electronics, both in terms of radiation dose and Single Event Effects. There is a single proton belt which contains highly energetic protons and affects the electronics in the region known as the South Atlantic Anomaly in the Earth’s low orbits. In addition, the electron belts are divided into two regions as inner and outer electron belts. In low Earth orbit, space systems pass through the inner belt electrons in SAA, and in high altitudes space systems pass through the outer belt electrons near the poles. Space systems which are either in the geostationary orbit or in the elliptical orbit pass through both inner and outer belts. The motion of all trapped particles is controlled by the Earth's magnetic field.

Galactic cosmic rays consist of protons and heavy ions with very high energies. Space systems in high Earth orbits are totally exposed to Galactic cosmic rays. However, space systems in low Earth orbits, the Earth's magnetic field shields some of those except at high latitudes. The flux of galactic cosmic rays are low. Therefore, they do not produce a serious source of radiation dose. However, heavy ions are very effective at causing single event effects.

Solar flare particles consists of protons and a few percent of heavy ions. Their energies are lower than galactic cosmic rays. The occurrence of solar flares is associated with the 11-year solar cycle. Major flares occur during the time of solar maximum and very intense particle fluxes are produced. Geostationary and other high altitude space systems are under threat in solar maximum. They may have the equivalent of a year's radiation dose in one major flare. Polar or other high inclination low Earth orbit space systems are under threat of these particles at high latitudes. Such as galactic cosmic rays, solar flare particles are very effective at causing single event effects.

The hardness assurance process begins with the definition of the radiation environment so that radiation induced damage levels can be estimated in advance. Radiation environment definitions are specific to the models that simulate the radiation effects for different environments. The estimate of fluxes in 500–700 km altitude has been performed by using trapped radiation belt, solar proton and heavy ions, galactic cosmic ray environment models. Since the estimate of fluxes has been assumed for solar solar minimum (2010), it is focused on three main sources.

a. Trapped protons in the inner radiation belt

b. Solar energetic particles

c. Protons and heavy ions from the Galactic cosmic rays.

The averaged electron and proton fluxes are analyzed for different altitudes (500–700 km) and inclinations ($28,5^0$, 60^0 and 90^0) as a function of energy. It is seen that the greatest inclination dependencies occur in $28,5^0$. For inclinations over $28,5^0$, the fluxes rise more gradually. 90^0 inclination has little effect on the flux levels. In addition, the largest altitude variations occurred in 500 km. For altitudes over 500 km, the flux increases gradually with increasing altitude. It is understood that the exposure of cosmic ray and solar flare particles gradually increases as altitude increases.

The space environment produces a great challenge to present and the future space systems. Defining the requirements claim the knowledge for the space environment and its effects on electronic systems as well as suitable risk estimate of the uncertainties.

Radiation hardness assurance is fully supported by simulation and analysis. The Monte Carlo based Geant4 simulation of the Sarayköy Gamma Irradiation Plant was used. Simulation of the irradiation gamma plant has been done by using Geant4 for the first time in Turkey. Geant4 has been used for the simulation of gamma rays in Gamma Irradiation Plant for performing analysis of radiation doses. The experimental and simulation results were validated by comparing the measured and the statistical particle transport. The results showed that experimental and simulation results are in good agreement, in spite of 12% of the statistical uncertainty of dosimeters and 8% of simulation. Monte Carlo radiation analysis supplies with a significant knowledge of the total ionizing dose.

The aging of the electronic parts are accelerated by radiation. This aging can lead to degradation of the electronic performance of the device [83]. Reduction on the performance of the electronic performance occurs as a functional failure at the device or its subsystems. Radiation Hardness Assurance is needed to ensure that the functionality or performance of the electronics during its system life is not compatible with the radiation environment.

In this thesis, only total ionizing dose and Single Event Effects hardening techniques are mentioned. Total ionizing dose testing is firstly done by exposing an electrical device to an ionizing radiation environment, and secondly by measuring the electrical performance of the device. Additionally, Single Event Effects testing is performed by continually measuring the device response while it is being irradiated. The device is electrically tested and the errors are counted during the irradiation.

For the tested components, it is understood that after 10 krad (100 Gy) both components tested according to the irradiation test plan lost their programming and is understood that the components can be used up to 3 krad. According to the dose rates calculated for 500–700 km altitude at different inclinations which is shown in Table A.3, this device can be used up to 2 years in 500 km altitude. However, to use this device in 600 km altitude and above is not possible. Also results from Single Event Effects test is showed that the device is susceptible to single event effects. The consequence of this loss of information due to upsets can occur.

As a last topic, in Europe there is a limited number of accelerator sites whose delivered ion beams fulfill the requirements of ESCC standards for SEE testing. A fully automatic dosimetry system to demonstrate the validity of beam characteristics of LNS sites were developed for SEE test as well as to accurately measure the parameters relevant to perform detailed SEE studies. With energies available at LNS and with four selected ions beams it is possible to perform SEE studies from few up to 110 $MeV.cm^2/mg$ of LET. The beam changing time is relatively short (few hours) and beam size and fluence are stable in time. Furthermore, the presence of air gives possibility to reach ”fine-tuned” LET values by adjusting the air thickness accordingly.

Last but not the least, operating the setup in air has its obvious advantages of reducing setup time and complexity.

REFERENCES

[1] Knoll, G., Radiation Detection and Measurement. John Wiley & Sons, New York, 1989.

[2] Nondestructive Testing and Evaluation Resource Center, `http://www.ndt-ed.org/EducationResources/CommunityCollege/Radiography/Physics/xrays.htm`, Last visited in June 2010.

[3] Tipler, P.A. Modern Physics, Worth Publishers Inc., New York, NY, 1978.

[4] John Hopkins University, Physics and Astronomy Department,`http://www.pha.jhu.edu/~c173_608/rutherford/rutherford.html`, Last visited in June 2010.

[5] Srour, J.R., Radiaiton Effects on Microelectronic in Space, Proc. IEEE, vol. 76, pp. 1443-1469, Nov. 1988.

[6] Tipler, P.A. Physics for Scientists and Engineers (4th ed.). Macmillan,. p. 511. ISBN 9781572594913, 1999.

[7] UC Davis ChemWiki by University of California, `http://chemwiki.ucdavis.edu/`, Last visited in June 2010.

[8] Mckelvey, J.P., Solid State and Semiconductor Physics, Harper and Row, New York, NY, 1966.

[9] The University of Hong Kong, Department of Physics, `http://www.physics.hku.hk/~phys0607/lectures/chap06.html`, Last visited in June 2010.

[10] Sears, F.W., University Physics, Addison-Wesley Publishing Co., Menlo Park, CA, 1982.

[11] Segre, E., Nuclei and Particles, W.A. Benjamin Inc., New York, NY, 1964.

[12] Hesston College, Physics Department, `http://www.hesston.edu/academics/faculty/nelsonk/2009/annihilaion-endeshaw/The_phenomenon_pair_production.htm`, Last visited in June 2010.

[13] Messenger, G.C. and Ash, M.S., *The Effects of Radiaiton on Electronic Systems.* Van Nostrand Reinhold, New York, 1986

[14] Ma, T.P., and Dressender P.V. eds., *Ionizing Radiation Effects in MOS Devices and Circuits.*, John Wiley & Sons, New York, 1989.

[15] Corliss, W.R., Space Radiation, United States Atomic Energy Commission Office of Information Services, 1968.

[16] Barth, J.L.,*Space,Atmospheric, and Terestial Radiation Environments*, IEEE Transactions on Nuclear Science, Vol. 50, No.3, 2003.

[17] Basu, S.; Antia, H.M., *Helioseismology and Solar Abundances.*, Physics Reports 457(5,6);217, 2008.

[18] Space Science News Archive, `http://spacescience.spaceref.com/newhome/headlines/images/sunspot1.jpg`, Last visited in June 2010.

[19] Bhat, B.R. and Sahu, R.P., *Radiation Shielding of Electronic Components in INSAT-2.*,Journal of Spacecraft Technology, Vol.3, 36, 1993.

[20] Johnson, F.S., *Satealite Environment Handbook*, Stanford University Press, California, 1965.

[21] Sagdeev, R.Z. and Kernel, C.F., *Collisionless Shock Waves*, Scientific American, pp 40-47, April, 1991.

[22] U.S. Centennial of Flight Commision, `http://www.centennialofflight.gov/essay/Dictionary/magnetosphere/DI70.htm`, Last visited in June 2010.

[23] Pike, C.P. et al., *A Correlation Study Relating Spacecarft Anomalies to Environmental Data*, Progress in Astronautics and Aeronautics, 47, 1976.

[24] Simpson, J.A., *Elemental and Isotropic composition of the Galactic Cosmic Rays*, Ann.Rev.Nucl.Sci.33, Page.323-381, 1983.

[25] Fleetwood, D.M., *Single event effects in systems using commercial electronics in harsh environments*, in IEEE NSRC Short Course, Tucson, AZ, July 1994.

[26] Barth, J., *Modeling Space Radiaiton Environment*, IEEE NSREC Short Course, NASA/Goddard Space Flight Center, 1997.

[27] Benton, E.V., "Space Radiation dosimetry in Low Earth orbit and beyond", Nucl. Instr. Meth. Phys. Res. B. 184, 255294.

[28] Tada, H.Y. and Carter, J.R., "Solar Cell Radiation Hand Book", NASA CR-155554, 1977.

[29] Hess, W.N.,"The Radiation Belt and Magnetosphere", Blaisdell Publishing Co., Waltham, 1968.

[30] Space Environment Information System, `http://www.spenvis.oma.be/help/background/traprad/motion.gif`, Last visited in June 2010.

[31] Wikipedia The Free Encyclopedia, `http://en.wikipedia.org/wiki/File:Van_Allen_radiation_belt.svg`, Last visited in June 2010.

[32] NCRP, "Guidance on Radiation Received in Space Activities", National Council on Radiaiton Protection and Measurements, Report 98.

[33] Tranquille, C. and Daily, E.J., "An Evaluation of Solar Proton Event Model for ESA Missions", ESA Journal, Vol. 16, 225, 1992.

[34] Poivey, C., "Radiation hardness assurance for space systems", SGT-Inc., National Aeronautics and Space Administration.

[35] Nasa Safety Standard, "Guidelines and Assesment Procedures for limiting Orbital Debris", NASA 1740, 14, August 1995.

[36] ”IADC Space Debris Mitigation Guidelines”, Inter-Agency Space Debris Coordination Committee, 15 October 2002.

[37] Velazco R. et al, ”Radiation Effects on Embedded Systems”, 1-9, Springer 2007.

[38] Petkov, M.P., The Effects of Space Environment on Electronic Components, BEACON eSpace at Jet Propulsion Laboratory, 2014/7913, 2003

[39] Pisacane, V.L., ”Fundamentals of Space Systems”, Oxford University Press, 2005.

[40] Sedra, A. and Smith, K., ”Microelectronic Circuits”, Oxford University Press,2004.

[41] Wall, J. and Macdonald, A., ”The NASA ASIC Guide: Assuring ASICS for Space”, Jet Propulsion Laboratory, California Institute of Technology and National Aeronautics and Space Administration, 1993.

[42] Web Page of Arnaldo J. Noyola, `http://ajnoyola.com/RHBD_primer.html`, Last visited in June 2010.

[43] NASA Thesaurus, ”Hierarchical Listing With Definitins”, Volume 1, NASA/SP-2009-7501/VOL1., 2009.

[44] Kolasinski et al. W.A., ”Simulation of cosmic-ray induced soft errors and latchup in integrated-circuit computer memories,” IEEE Trans. on Nuclear Science, vol. NS-26, no. 6, pp. 5087-5091, 1979.

[45] Nichols, D.K. et al., ”An observation of proton-induced latchup,” IEEE Trans. on Nuclear Science, vol. 39, no. 6, pp. 1654-1656, 1992.

[46] Adams, L. et al., ”A verified proton induced latchup in space,” IEEE Trans on Nuclear Science, vol. 39, no. 6, pp. 1804-1808, Dec. 1992.

[47] Wikipedia The Free Encyclopedia, `http://en.wikipedia.org/wiki/Radiation_hardening`, Last visited in June 2010.

[48] Mouret, I. et al., ”Temperature and angular dependence of substrate response in SEGR,” IEEE Trans. on Nuclear Science, vol. 41, no. 6, pp. 2216-2221, 1994.

[49] Mouret, I. et al., ”Experimental evidence of the temperature and angular dependence in SEGR,” Proceedings of the Third European Conference on Radiation and its Effects on Components and Systems (RADECS), Arcachon, France, Sept. 1995.

[50] Johnson, G.J. et al., ”Simulating single-event burnout in n-channel power MOSFETs,” IEEE Trans. on Electron Devices, vol. 40, pp. 1001-1008, 1993.

[51] LaBel, K., ”Single event effects specification”, website: http://radhome.gsfc.nasa.gov/radhome/papers/seespec.htm, 1993.

[52] NASA/GSFC Radiation Effects & Analysis Home Page, `http://radhome.gsfc.nasa.gov/radhome/images/seeca4c.gif`, Last visited in June 2010.

[53] The Aerospace Corporation, `http://www.aero.org/capabilities/seet/images/LETcurve.gif`, Last visited in June 2010.

[54] Vette, J.I., ”The AE8 Trapped Electron Model Environment”, NSSDC/WDC-A-R&S 9124, NASAGSFC, 1991.

[55] Sawyer, D.M., and Vette, J.I., ”AP8 Trapped Proton Environment for Solar Maximum and Solar Minimum”, NSSDC/WDC-A-R&S 7606, NASAGSFC, 1976.

[56] European Cooperation for Space Standardization, ECSS-E-ST-10-04C,”Space Engineering–Space Environment”, Noordwijk, The Netherlands, November 2008.

[57] Heynderickx, D., Kruglanski, M., Pierrard, V., Lemaire, J., Looper, M. D. and Blake, J. B., ”A low altitude trapped proton model for solar minimum conditions based on SAMPEX/PET data,” IEEE Trans. Nucl. Sci., vol. 46, no. 6, 1999.

[58] Huston, S. L., ”Space Environments and Effects: Trapped Proton Model”, NASA/CR-2002-211784, 2002.

[59] Boscher, D. M., Bourdarie, S. A., Friedel, R. H. W. and Belian, R. D., ”Model for the geostationary electron environment: POLE”, IEEE Trans. Nucl. Sci., vol. 50, no. 6, pp. 2278-2283, 2003.

[60] Huston, S. L. and Pfitzer, K. A., ”Space Environment Effects: Low- Altitude Trapped Radiation Model”, NASA/CR-1998-208593, 1998.

[61] Gussenhoven,M. S., Mullen, E. G., Violet, M. D., Hein, C., Bass, J. and Madden, D., ”CRRES high energy proton flux maps”, IEEE Trans. Nucl. Sci., vol. 40, no. 6, pp. 1450-1457, 1993.

[62] Wrenn, G. L., Rodgers, D. J. and Buehler, P., ”Modeling the outer belt enhancements of penetrating electrons”, J. Spacecraft Rockets, vol. 37, no. 3, pp. 408-415, 2000.

[63] Brautigam, D. H., Gussenhoven, M. S., Mullen, E. G., ”Quasi-static model of outer zone electrons”, IEEE Trans. Nucl. Sci., vol. 39, no. 6, 1992

[64] Lauenstein, J.M., Barth, J.L., ” Radiation belt modeling for spacecraft design: model comparisons for common orbits”, Radiation Effects Data Workshop, IEEE, Pages 102 - 109, 2005.

[65] King, J. H., Solar Proton Fluences for 1977-1983 Space Missions, J. Spacecraft Rockets, 11, 401, 1974.

[66] Feynman, J., G. Spitale, J. Wang, and S. Gabriel, Interplanetary Proton Fluence Model: JPL 1991, J. Geophys. Res., 98, 13,281-13,294, 1993.

[67] Xapsos, M. A., G. P. Summers, J. L. Barth, E. G. Stassinopoulos, and E. A. Burke, Probability Model for Worst Case Solar Proton Event Fluences, IEEE Trans. Nucl. Sci., 46, 1481-1485, 1999.

[68] Xapsos, M. A., G. P. Summers, J. L. Barth, E. G. Stassinopoulos, and E. A. Burke, Probability Model for Cumulative Solar Proton Event Fluences, IEEE Trans. Nucl. Sci., 47, 486-490, 2000.

[69] Stassinopoulos, E. G., SOLPRO: A Computer Code to Calculate Probabilistic Energetic Solar Proton Fluences, NSSDC 75-11, Greenbelt, Maryland, 1975.

[70] A.J. Tylka et al., ”CREME96: A Revision of the Cosmic Ray Effects on Micro- Electronics Code”, IEEE Transactions on Nuclear Science 44, 2150-2160 (1997).

[71] Adams, J. H., ”Cosmic Ray Effects on Microelectronics, Part IV”, Naval Research Laboratory, Washington DC 20375–5000, USA, 1986.

[72] Peyrard P.F. et al., ”OMERE 2.0 A Toolkit For Space Environment”, Proceedings of RADECS 2003, Radiation and Its Effects on Components and Systems, Noordwijk, The Netherlands, 15-19 September 2003, (ESA SP-536, The Netherlands)

[73] Geant4, `http://geant4.web.cern.ch/`, Last visited in June 2010.

[74] TAEK, `http://www.taek.gov.tr/`, Last visited in June 2010.

[75] The European Cooperation for Space Standardization, `http://www.ecss.nl/`, Last visited in June 2010.

[76] Mc Lean, F and Oldham, T., ”Basic Mechanisms of Radiation Effects on Electronic Materials, Devices and Integrated Circuits”, IEEE NSREC Short Course, Snowmass, July 1987.

[77] Total Dose Steady State Irradiation test Method. ESA/SCC Basic Specification No: 22900. Edited by ESA.

[78] Istituto Nazionale di Fisica Nucleare, `http://www.lns.infn.it`, Last visited in June 2010.

[79] SingleEvent Effects Test Methods and Guidelines. ESA/SCC basic specification No: 25100. Edited by ESA.

[80] Petersen, E.L., Pickel, J.C., Adams, J.H., Jr. and Smith, E.C., Jr., Rate Prediction for Single Event Effects–A Critique, IEEE Transactions on Nuclear Science , NS-39, Dec 1992, pp 1577-99.

[81] SELDP: An instrument for the automatic detection and protection from SEL during beam tests. Proceedings of RADECS Workshop 2002 pp.4

[82] Harboe-Sorensen, R., Guerre, F.-X. and Roseng, A., ”Design, Testing and Calibration of a Reference SEU Monitor System.” Proceedings of RADECS 2005.

[83] Barth, J.L., LaBel, A.K., Poivey C., ”Radiation Assurance For the Space Environment”, IEEE International Conference on Integrated Circuit Design and Technology, Austin TX, May 2004.

APPENDIX A

TABLES

A.1 TRAPPED PARTICLE FLUXES

A.1.1 Trapped Electron Fluxes in Solar Minimum

Table A.1: Integrated trapped electron fluxes in 500–700 km altitudes for solar minimum.

	500 km			600 km			700 km		
Energy (MeV)	Inclination 28,5	60,00	90,00	Inclination 28,5	60,00	90,00	Inclination 28,5	60,00	90,00
0,04	7,6299E+03	6,5099E+04	1,4223E+05	6,3814E+04	2,7710E+05	2,2852E+05	1,8954E+05	4,2199E+05	3,4303E+05
0,10	4,9988E+03	3,8778E+04	8,7358E+04	4,4532E+04	1,7098E+05	1,4189E+05	1,3213E+05	2,6338E+05	2,1567E+05
0,25	1,0816E+03	1,0906E+04	2,6469E+04	1,3432E+04	4,8650E+04	4,1851E+04	4,0172E+04	7,4250E+04	6,3029E+04
0,50	1,9371E+02	3,8036E+03	7,6242E+03	1,0934E+03	1,2074E+04	1,0662E+04	3,2184E+03	1,6292E+04	1,4351E+04
0,75	6,5969E+01	2,0564E+03	3,8096E+03	3,2785E+02	5,9254E+03	5,1823E+03	9,3115E+02	7,7414E+03	6,7867E+03
1,00	3,3767E+01	1,2938E+03	2,3421E+03	1,4913E+02	3,6384E+03	3,1539E+03	4,1766E+02	4,6959E+03	4,0900E+03
1,50	1,2464E+01	5,4440E+02	1,0185E+03	5,5325E+01	1,6222E+03	1,3637E+03	1,5281E+02	2,0767E+03	1,7557E+03
2,00	5,6812E+00	2,4760E+02	4,4099E+02	2,4920E+01	7,1503E+02	5,8915E+02	6,8236E+01	9,1277E+02	7,5656E+02
2,50	2,6650E+00	1,1529E+02	1,9876E+02	1,1587E+01	3,2772E+02	2,6496E+02	3,1447E+01	4,1690E+02	3,3953E+02
3,00	0,0000E+00	5,1495E+01	7,8013E+01	2,1587E+00	1,2900E+02	1,0240E+02	5,8193E+00	1,6193E+02	1,2970E+02
3,50	0,0000E+00	2,3569E+01	3,0157E+01	0,0000E+00	5,0278E+01	3,9318E+01	0,0000E+00	6,2657E+01	4,9342E+01
4,00	0,0000E+00	9,9026E+00	1,0209E+01	0,0000E+00	1,7356E+01	1,3289E+01	0,0000E+00	2,1611E+01	1,6593E+01
4,50	0,0000E+00	3,5129E+00	3,0426E+00	0,0000E+00	5,2889E+00	3,9674E+00	0,0000E+00	6,5814E+00	4,9269E+00
5,00	0,0000E+00	1,1203E+00	0,0000E+00	0,0000E+00	1,5242E+00	1,1030E+00	0,0000E+00	1,9059E+00	1,3597E+00
5,50	0,0000E+00	0,0000E+00	0,0000E+00	0,0000E+00	0,0000E+00	0,0000E+00	0,0000E+00	0,0000E+00	0,0000E+00
6,00	0,0000E+00	0,0000E+00	0,0000E+00	0,0000E+00	0,0000E+00	0,0000E+00	0,0000E+00	0,0000E+00	0,0000E+00
6,50	0,0000E+00	0,0000E+00	0,0000E+00	0,0000E+00	0,0000E+00	0,0000E+00	0,0000E+00	0,0000E+00	0,0000E+00
7,00	0,0000E+00	0,0000E+00	0,0000E+00	0,0000E+00	0,0000E+00	0,0000E+00	0,0000E+00	0,0000E+00	0,0000E+00

A.1.2 Trapped Proton Fluxes in Solar Minimum

Table A.2: Integrated trapped proton fluxes in 500–700 km altitude for solar minimum.

	500 km			600 km			700 km		
Energy	Inclination			Inclination			Inclination		
(MeV)	28,5	60,00	90,00	28,5	60,00	90,00	28,5	60,00	90,00
0,10	3,4104E+01	2,0308E+03	1,1109E+03	8,8121E+01	4,2093E+03	2,1217E+03	1,9424E+02	7,5754E+03	3,9131E+03
0,25	3,3648E+01	9,6470E+02	5,5944E+02	8,7041E+01	1,9159E+03	1,0304E+03	1,9218E+02	3,3718E+03	1,8042E+03
0,50	3,3161E+01	4,4193E+02	2,7377E+02	8,5923E+01	8,3140E+02	4,9107E+02	1,9008E+02	1,4323E+03	8,1765E+02
0,75	3,2733E+01	2,7562E+02	1,7851E+02	8,4937E+01	5,0624E+02	3,1914E+02	1,8814E+02	8,6336E+02	5,2131E+02
1,00	3,2352E+01	2,0142E+02	1,3480E+02	8,4090E+01	3,6681E+02	2,4177E+02	1,8647E+02	6,2162E+02	3,9207E+02
2,00	3,1896E+01	1,0278E+02	7,4175E+01	8,3008E+01	1,8995E+02	1,3655E+02	1,8414E+02	3,2089E+02	2,2349E+02
3,00	3,1559E+01	7,3615E+01	5,4890E+01	8,2112E+01	1,3853E+02	1,0354E+02	1,8192E+02	2,3533E+02	1,7192E+02
4,00	3,1227E+01	5,7100E+01	4,3726E+01	8,1228E+01	1,0968E+02	8,4481E+01	1,7974E+02	1,8771E+02	1,4238E+02
5,00	3,0906E+01	4,8684E+01	3,7888E+01	8,0339E+01	9,4933E+01	7,4379E+01	1,7746E+02	1,6334E+02	1,2661E+02
6,00	3,0589E+01	4,2795E+01	3,3745E+01	7,9460E+01	8,4536E+01	6,7157E+01	1,7520E+02	1,4610E+02	1,1525E+02
8,00	2,9910E+01	3,6383E+01	2,9101E+01	7,7604E+01	7,2957E+01	5,8868E+01	1,7061E+02	1,2661E+02	1,0187E+02
10,00	2,9247E+01	3,2786E+01	2,6447E+01	7,5732E+01	6,6266E+01	5,3922E+01	1,6622E+02	1,1528E+02	9,3775E+01
12,00	2,8711E+01	3,0751E+01	2,4921E+01	7,4219E+01	6,2400E+01	5,1011E+01	1,6238E+02	1,0856E+02	8,8824E+01
15,00	2,7937E+01	2,8376E+01	2,3109E+01	7,2024E+01	5,7783E+01	4,7473E+01	1,5683E+02	1,0047E+02	8,2710E+01
17,00	2,7431E+01	2,7287E+01	2,2267E+01	7,0591E+01	5,5614E+01	4,5792E+01	1,5345E+02	9,6709E+01	7,9797E+01
20,00	2,6698E+01	2,5851E+01	2,1147E+01	6,8506E+01	5,2713E+01	4,3527E+01	1,4853E+02	9,1658E+01	7,5835E+01
25,00	2,5694E+01	2,4276E+01	1,9896E+01	6,5763E+01	4,9586E+01	4,1054E+01	1,4224E+02	8,6305E+01	7,1560E+01
30,00	2,4745E+01	2,2909E+01	1,8802E+01	6,3159E+01	4,6834E+01	3,8857E+01	1,3625E+02	8,1556E+01	6,7722E+01
35,00	2,3798E+01	2,1698E+01	1,7812E+01	6,0601E+01	4,4407E+01	3,6863E+01	1,3066E+02	7,7487E+01	6,4416E+01
40,00	2,2895E+01	2,0578E+01	1,6895E+01	5,8160E+01	4,2152E+01	3,5004E+01	1,2532E+02	7,3691E+01	6,1321E+01
45,00	2,2033E+01	1,9537E+01	1,6042E+01	5,5829E+01	4,0050E+01	3,3266E+01	1,2022E+02	7,0138E+01	5,8414E+01
50,00	2,1209E+01	1,8570E+01	1,5246E+01	5,3602E+01	3,8083E+01	3,1638E+01	1,1534E+02	6,6802E+01	5,5679E+01
60,00	1,9434E+01	1,6660E+01	1,3688E+01	4,9052E+01	3,4283E+01	2,8505E+01	1,0560E+02	6,0403E+01	5,0393E+01
70,00	1,7823E+01	1,4894E+01	1,2241E+01	4,4896E+01	3,0767E+01	2,5606E+01	9,6577E+01	5,4460E+01	4,5484E+01
80,00	1,6359E+01	1,3347E+01	1,0973E+01	4,1114E+01	2,7667E+01	2,3043E+01	8,8377E+01	4,9184E+01	4,1116E+01
90,00	1,4915E+01	1,1887E+01	9,7747E+00	3,7476E+01	2,4760E+01	2,0639E+01	8,0547E+01	4,4252E+01	3,7022E+01
100,00	1,3618E+01	1,0608E+01	8,7250E+00	3,4179E+01	2,2194E+01	1,8513E+01	7,3452E+01	3,9870E+01	3,3379E+01
125,00	1,0595E+01	7,8927E+00	6,4836E+00	2,6657E+01	1,6755E+01	1,3987E+01	5,7483E+01	3,0508E+01	2,5582E+01
150,00	8,2703E+00	5,9203E+00	4,8560E+00	2,0837E+01	1,2729E+01	1,0632E+01	4,5091E+01	2,3470E+01	1,9707E+01
175,00	6,4708E+00	4,4676E+00	3,6592E+00	1,6319E+01	9,7184E+00	8,1218E+00	3,5440E+01	1,8134E+01	1,5244E+01
200,00	5,0702E+00	3,3887E+00	2,7704E+00	1,2800E+01	7,4507E+00	6,2299E+00	2,7898E+01	1,4062E+01	1,1833E+01
300,00	1,8183E+00	1,1634E+00	0,0000E+00	4,7013E+00	2,6489E+00	2,2129E+00	1,0623E+01	5,2268E+00	4,4118E+00

A.1.3 Dose in Different Altitudes and Inclinations

Table A.3: Dose values in different altitutes between 500 km – 700 km altitudes.

	Altitudes				
	500	550	600	650	700
Inclination (degree)	Average dose (krad /year)	Average dose (krad /year)	Average dose (krad /year)	Average dose (krad /year)	Average dose (krad /year)
98	1,157E-01	1,745E-01	2,486E-01	3,391E-01	4,503E-01
93	1,147E-01	1,729E-01	2,460E-01	3,356E-01	4,449E-01
88	1,140E-01	1,717E-01	2,451E-01	3,345E-01	4,444E-01
83	1,150E-01	1,732E-01	2,472E-01	3,380E-01	4,485E-01
78	1,172E-01	1,766E-01	2,522E-01	3,443E-01	4,572E-01
73	1,210E-01	1,826E-01	2,600E-01	3,548E-01	4,716E-01
68	1,264E-01	1,911E-01	2,720E-01	3,710E-01	4,931E-01
63	1,338E-01	2,020E-01	2,893E-01	3,948E-01	5,241E-01
58	1,449E-01	2,189E-01	3,148E-01	4,295E-01	5,702E-01
53	1,652E-01	2,499E-01	3,556E-01	4,847E-01	6,407E-01

Inclination (degree)	Average dose (Gy / year)	Average dose (Gy / year)	Average dose (Gy / year)	Average dose (Gy / year)	Average dose (Gy / year)
98	1,157	1,745	2,486	3,391	4,503
93	1,147	1,729	2,460	3,356	4,449
88	1,140	1,717	2,451	3,345	4,444
83	1,150	1,732	2,472	3,380	4,485
78	1,172	1,766	2,522	3,443	4,572
73	1,210	1,826	2,600	3,548	4,716
68	1,264	1,911	2,720	3,710	4,931
63	1,338	2,020	2,893	3,948	5,241
58	1,449	2,189	3,148	4,295	5,702
53	1,652	2,499	3,556	4,847	6,407

APPENDIX B

CODES

B.1 tgipsource.mac

```
/random /resetEngineFrom currentEvent.rndm
/control/saveHistory
/control/verbose 0
/run/verbose 0
/event/verbose 0
/tracking/verbose 0

#B1
/tgip/det/tallyPosition 332.0 -282.3 -160. cm

#A2
/tgip/det/tallyPosition 332.0 -282.3 -169 cm

#A1
/tgip/det/tallyPosition 336.6 -274.3 -160. cm

#A3
/tgip/det/tallyPosition 336.6 -274.8 -170. cm

/tgip/det/update
/run/initialize
/gps/source/intensity 1.
/gps/particle gamma
/gps/pos/type Beam
```

```
#The incident surface is in the y-z plane

/gps/pos/rot1 0 1 0
/gps/pos/rot2 0 0 1
/gps/pos/shape Rectangle
/gps/pos/centre -67.5 20. -185. cm
/gps/pos/halfx 432.5 mm
/gps/pos/halfz 475.0 mm\\

#The beam is traveling along the x-axis

/gps/ang/rot1 0 0 1
/gps/ang/rot2 0 1 0
/gps/ang/type cos

/gps/ang/mintheta 45. deg
/gps/ang/maxtheta 135. deg

/gps/ang/minphi 139. deg
/gps/ang/maxphi 141. deg

/gps/ene/mono 1.17 MeV
/gps/source/add 0.5
/gps/particle gamma
/gps/pos/type Beam

#The incident surface is in the y-z plane

/gps/pos/rot1 0 1 0
/gps/pos/rot2 0 0 1
/gps/pos/shape Rectangle
/gps/pos/centre -67.5 20. -185. cm
/gps/pos/halfx 432.5 mm
/gps/pos/halfz 475.0 mm

#The beam is traveling along the x-axis
```

```
/gps/ang/rot1 0 0 1
/gps/ang/rot2 0 1 0

/gps/ang/type cos
/gps/ang/mintheta 45. deg

/gps/ang/maxtheta 135. deg
/gps/ang/minphi 139. deg

/gps/ang/maxphi 141. deg
/gps/ene/mono 1.33 MeV

/tgip/event/printModulo 1000
/tgip/stepMax 0.01 mm

/run/beamOn 1000000
```

B.2 tgip.cc

```
#include "G4RunManager.hh"
#include "G4UImanager.hh"

#include "G4UIterminal.hh"
#include "G4UItcsh.hh"

#include "Randomize.hh"
#include "DetectorConstruction.hh"

#include "PhysicsList.hh"
#include "PrimaryGeneratorAction.hh"

#include "RunAction.hh"
#include "EventAction.hh"

#include "TrackingAction.hh"
```

```
#include "SteppingAction.hh"

#include "SteppingVerbose.hh" #ifdef G4UI\_USE_ROOT

#include "G4UIRoot.hh"
#endif

#ifdef G4VIS_USE #include "G4VisExecutive.hh" #endif

int main(int argc,char** argv) {

  // Choose the Random engine
  CLHEP::HepRandom::setTheEngine(new CLHEP::RanecuEngine);

  //my Verbose output class
  G4VSteppingVerbose::SetInstance(new SteppingVerbose);

  // Construct the default run manager
  G4RunManager * runManager = new G4RunManager;

  // Set mandatory initialization classes
  DetectorConstruction* det;
  PhysicsList* phys;
  PrimaryGeneratorAction* kin;
  EventAction* evt;
  runManager-$>$SetUserInitialization(det = new DetectorConstruction);
  runManager-$>$SetUserInitialization(phys = new PhysicsList);
  runManager-$>$SetUserAction(kin = new PrimaryGeneratorAction(det));

#ifdef G4VIS_USE

  // Visualization manager

  G4VisManager* visManager = new G4VisExecutive;
  visManager->Initialize();
#endif
```

```
  // Set user action classes

  RunAction* run;
  runManager->SetUserAction(run = new RunAction(det,phys,kin));
  runManager->SetUserAction(new EventAction(det));
  runManager->SetUserAction(new TrackingAction(run));
  runManager->SetUserAction(new SteppingAction(det,run,kin,evt));

  // Initialize G4 kernel
  runManager->>Initialize();

  // Get the pointer to the User Interface manager
  G4UImanager* UI = G4UImanager::GetUIpointer();

  // Define UI terminal for interactive mode
  if (argc==1)
    {
     G4UIsession* session = 0;

#if defined (G4UI_USE_ROOT)

  // G4URoot is a ROOT based GUI.

  session = new G4UIRoot(argc,argv);
#else

#ifdef G4UI_USE_TCSH
  session = new G4UIterminal(new G4UItcsh);
#else
  session = new G4UIterminal();
#endif
#endif

    UI->ApplyCommand("/control/execute vis.mac");
    session->SessionStart();
    delete session;
  }
```

```
 else

  // Batch mode

  {
    G4String command = "/control/execute ";
    G4String fileName = argv[1];
    UI->ApplyCommand(command+fileName);
  }

  // Job termination

#ifdef G4VIS_USE
  delete visManager;
#endif
  delete runManager;
  return 0;
}
```

CURRICULUM VITAE

PERSONAL INFORMATION

Surname, Name: Amutkan, Özge
Nationality: Turkish (TC)
Date and Place of Birth: 1 May 1979, Ankara
Phone: +90 312 210 43 31
email: e141155@metu.edu.tr

EDUCATION

Fall 2003- Present Ph.D. Program, Middle East Technical University (METU), Ankara
M.Sc: Ankara University, The Graduate School of Natural and Applied Sciences, Physics Engineering, February 2003.
B.S.: Ankara University, The Faculty of Education, Department of Physics Engineering, June 2001.
High School: Ankara Kurtuluş Lisesi, Ankara, 1997.

PUBLICATIONS

1. Alpat,B., Menichelli,M., Amutkan,O. et. al., 'The Radiation Hardness Assurance Facility at INFN-LNS Catania for the Irradiation of Electronic Components in Air', RADECS, Paper Number 1112, 2009.
2. Alpat, B., Menichelli,M., Amutkan,O. et. al., 'Irradiation Facility at INFN-LNS Catania for Radiation Hardness Assurance Tests in Air., Heavy Ions in

Therapy and Space Symposium, 2009. (It will be published in Radiation and Environmental Biophysics.)

PROCEEDINGS

1. Alpat,B., Menichelli,M., Amutkan,O. et. al., 'The Radiation Assurance Test Facility at INFN-LNS Catania', HIAT09, 11. International Conference on Heavy Ions Accelerator Technology, 2009.

RESEARCH EXPERIENCES

- 2007 - Present, Research Assistant, ”Development High Resolution Electro - Optic Camera Technology” Project, METU, Ankara.
- 2008 - 2009, Researcher, Radiation Hardness Assurance Tests, Istituto Nazionale di Fisica Nucleare, Perugia, Italy.
- 2002 Summer Student, Summer Student Program in Deutsches Elektronen - Synchrotron DESY, Germany.
- 2000 Trainee, Ankara Nuclear Research and Education Center, Ankara.